Appendix 6.

Aeronomy of Ice in the Mesosphere (AIM) Mission

Project Data Management Plan (PDMP)

Signature Page

Aeronomy of Ice in the Mesosphere (AIM) **Project Data Management Plan**	
Jerry Jason, AIM Project Manager	Date:
Scott Bailey, AIM Principal Investigator	Date:
Cora Randall, CIPS Principal Investigator	Date:
Mark Hervig, SOFIE Principal Investigator	Date:
Robert M. Candey, Archive Project Scientist	Date
Esayas Shume, HQ Program Scientist	Date
By signing this document, signatories are certifying that the content herein is acceptable direction for managing the project's data and that they will ensure its implementation by those over whom they have authority.	

Change History Log		
Revision	**Effective Date**	**Description of Changes (Reference the CCR & CCB/ERB Approval Date)**
Version 1	4/22/2020	Original
Version 2	11/01/2022	Updated Sections 1.3, 1.4, 1.5, 2.1, 2.2, 3.1.2.1, 3.2.1, 4.2.1, 4.1.2, 4.3.2, 6.1, 6.2, 7.4, 8.

Aeronomy of Ice in the Mesosphere (AIM)

Project Data Management Plan

1. Introduction

The AIM satellite was launched on April 25, 2007 as part of NASA's Heiophysics System Observatory (HSO) to study polar mesospheric clouds (PMCs) and the environment in which they form. PMCs (known alternately as noctilucent clouds, NLCs) consist of ice particles which exist near and below the polar summer mesopause (~83 km). The seasonal appearance of these clouds is associated with upwelling in the polar summer mesosphere which simultaneously lowers temperatures and enhances water vapor. PMCs are considered to respond to solar variability [*Garcia*, 1989], increasing greenhouse gases (GHG) [*Thomas*, 1996], meteoric influx [*Hervig et al.*, 2012], space vehicle traffic [*Stevens et al.*, 2012], meteorology in the polar winter [*Karlsson et al.*, 2007], forcing from the stratosphere [*Lübken et al*., 2009], and tidal variations [*Fiedler et al.*, 2005; 2011]. PMCs garnered considerable interest due to reports that they were increasing and moving equatorward during recent decades. These changes were anticipated due to rising greenhouse gases, particularly CO_2 and CH_4. Rising CO_2 cools the stratosphere and mesosphere and CH_4 oxidizes in the upper atmosphere to produce H_2O, changes that should enhance PMCs. The original overall AIM goal was to resolve why PMCs form and why they vary. These objectives were met by measuring PMCs and the thermal, chemical and dynamical environment in which they form. The results were used to quantify the connection between PMCs and the meteorology of the polar mesosphere, ultimately providing a basis for relating PMCs to changing global climate [*Hervig et al*., 2016]. The AIM measurement capabilities and science goals have evolved since the original proposal, to encompass measurements of global dynamics including gravity waves and planetary waves, and observations of meteoric particles in the mesosphere and stratosphere.

1.1. Purpose and Scope

This document describes the AIM Science Data System (SDS), its structure, its policies and its products, including:

- Information for users about the SDS, including an overview of what products are available and how access is provided;
- Guidelines and specific technical information to the SDS implementation teams to aid in construction of the data system;
- Information useful for evaluation of the SDS by AIM program management and the NASA Data System review team.

Additional details concerning the SDS are sometimes contained in referenced documents.

1.2. Plan Development, Maintenance, and Management Responsibility

This document is produced and maintained by the CIPS and SOFIE instrument Principal Investigators and their respective data management team members, with approval from the AIM Principal Investigator.

1.3. Change Control

This document replaces and supersedes the AIM Data Management Plan Version 2 (aim_dmp_v2.doc) and all preceding Aim Mission Archive Plans. The major milestones of the Data Management Plan are:

- 1 - This preliminary version was used as a planning tool during mission design. The SDS manager made changes during this time when necessary. Concurrence signatures were obtained by the time of the Preliminary Design Review.
- 2 - This was the first signed version of this document and was subject to standard change control procedures. It was available for signature at the Mission Critical Design Review.
- 3 - This version was signed and available approximately 6 months before the AIM spacecraft is launched.
- 4 - AIM Mission Archive Plans – As per the Heliophysics Data Policy, information in the AIM DMP version 2 was superseded by the Mission Archive Plans(MAP)s included in each senior Review from 2009 through 2017. These MAPs included details of the status of data availability and archiving plans.
- 5 - PDMP Version 1. This is the initial version and was available for the 2020 Senior Review. This version reflects up to date information regarding changes that have been made to accommodate flight operations as well as the new science objectives.
- 6 - PDMP Version 2. This is the first major revision (this document), which is signed and available for the 2023 Senior Review.

1.4. About This Document

Section 2 is the AIM mission overview and describes:

- 2.1. Mission Objectives
- 2.2. Launch, Orbit, and Operations

Section 3 describes each instrument on AIM:

- 3.1. The Cloud Imaging and Particle Size (CIPS) Experiment
- 3.2. The Solar Occultation For Ice Experiment (SOFIE)
- 3.3. The Cosmic Dust Experiment (CDE)

Section 4 describes the data products produced by the AIM mission.

Section 5 describes the ground system that project data is routed through.

Section 6 provides detail on the transfer of data between flight and ground mission elements.

Section 7 describes the process for archiving AIM data and how those archives may be accessed.

Section 8 lists the references.

1.5. Relevant Documents

This section identifies other project/mission documentation with higher-level guiding requirements or that provide more detail or context (see Table 1.5).

Table 1.5. Relevant AIM Documents		
Title	**Document Number or Location**	**Publication Date**
AIM Science Data System Interface Control Document	aim_sds_icd_040105.doc aim.hamptonu.edu	1 April 2005
AIM Data Management Plan V2	aim_dmp_v2.doc aim.hamptonu.edu	12 February 2007

2. Mission Overview

AIM was the first satellite mission dedicated to the study of PMCs, with the overall goal to resolve why PMCs form and why they vary. The AIM experiment includes three instruments: SOFIE (Solar Occultation For Ice Experiment), a solar occultation differential absorption radiometer covering ultraviolet (UV) through infrared (IR) wavelengths; CIPS (Cloud Imaging and Particle Size experiment), a panoramic UV imager; and CDE (Cosmic Dust Experiment), an in-situ cosmic dust detector.

2.1. Mission Objectives

PMCs are Earth's highest clouds, occupying the atmospheric region near the high-latitude summer mesopause at ~ 83 km. They typically extend from ~ 55° latitude to the geographic pole, occurring in each summer in both hemispheres between about mid-May to mid-August in the North and mid-November to mid-February in the South. The polar upper mesosphere becomes the coldest place on earth around summer solstice, when the temperature plummets below 130K. Known as noctilucent, or "night-shining" clouds (NLCs) as seen by ground based observers, their name derives from the fact that they are seen at evening or morning twilight, when the lower atmosphere is in darkness, but the upper atmosphere is still sunlit. First identified over 120 years ago [*Leslie*, 1885], their nature as water-ice particles was not confirmed observationally until relatively recently [*Hervig et al.*, 2001]. There is great interest in PMCs because they are changing in ways that are not understood. They are occurring more frequently, becoming brighter and seem to be appearing at lower latitudes than ever before [*Deland et al.*, 2006, 2007; *Taylor et al*., 2002]. This behavior suggests a possible connection with global change occurring at lower altitudes.

The original overall goal of AIM was to resolve why PMCs form and why they vary. The original six science objectives were designed to address the mission goal. The first objective was to understand the cloud microphysics, i.e. the relationship between temperature, water vapor and size distribution under a variety of conditions and times in the PMC season, and for different cloud types. The second objective was focused on assessing the role of atmospheric gravity waves in PMC formation. It is clear that waves are important because their presence is obvious in the many ground-based photographs of the clouds. The third objective addressed the question of the influence of temperature in controlling the length of the PMC season. Clearly, extremely low temperatures (on the order of 140K or less) are essential because where the clouds form ~ 83 km above the surface, the pressure is one hundred thousand times less than at the surface and the air may be as much as a million times drier than surface desert air. The fourth objective addressed upper mesosphere H_2O chemistry and how it changes during the PMC season. As noted earlier, the clouds are known to be made up of water ice crystals and interactions between H_2O and O_3 and the role of solar Lyman-α radiation which controls H_2O at the cloud altitude needs to be

understood. The fifth objective was to assess the sources of seed particles needed for PMC formation by providing a nucleation site to begin the particle growth process. The last objective combined results from the first five to validate coupled chemistry, dynamics and PMC microphysical models and to assess the ability to quantify long-term changes, and predict future changes in PMCs based on these models, historical data sets and AIM results.

AIM measurements continue to have strong impacts on our understanding of the structure and behavior of the upper atmosphere, including detailed knowledge of meteoric particles, as well as atmospheric waves, their interactions with PMCs, and their role in global atmospheric coupling. The evolution in our understanding since AIM was first proposed 17 years ago is striking. The initial mission was sharply focused on the PMC layer at ~84 km altitude, with the goal being to understand why PMCs form and how they vary. Our new understanding reveals an atmosphere that is strongly coupled in altitude, latitude, longitude and across hemispheres. These paradigm changes are reflected in the progression of AIM science objectives (SO) from the original mission to the subsequent extended missions, as summarized below.

Original Mission Science Objectives:

- SO-1. What is the global morphology of PMC particle size, occurrence frequency and dependence upon H_2O and temperature?
- SO-2. Do GWs enhance PMC formation by perturbing the required temperature for condensation and nucleation
- SO-3. How does dynamical variability control the length of the cold summer mesopause season, its latitudinal extent and possible interhemispheric asymmetry?
- SO-4. What are the relative roles of gas phase chemistry, surface chemistry, condensation/sublimation and dynamics in determining the variability of water vapor in the polar mesosphere?
- SO-5. Is PMC formation controlled solely by changes in the frost point or do extraterrestrial forcings such as cosmic dust influx or ionization sources play a role?
- SO-6. What is needed to establish a physical basis for the study of mesospheric climate change and its relationship to global change?

2010 Extended Mission Science Objectives:

- SO-1. Are there temporal variations in PMCs that can be explained by changes in solar irradiance and particle input?
- SO-2. What processes are responsible for north/south differences in PMC features?
- SO-3. What governs the interannual variability in PMCs?
- SO-4. What is the mechanism of teleconnection between winter temperatures and summer hemisphere PMC's?
- SO-5. What is the AIM capability to measure gravity waves outside the PMC domain?

2013 Extended Mission:

- SO-1. How are PMC variations indicative of the dynamics of the whole atmosphere?
- SO-2. How does changing solar irradiance affect PMCs and the environment in which they form?

- SO-3. What is the response of PMCs and their environment to changing atmospheric composition resulting from terrestrial
- forcing?
- SO-4. What are the drivers behind changing atmospheric circulation as Indicated by meteoric smoke observations?
- SO-5. What is the effect of rapidly transported launch vehicle exhaust on PMC variability during the unique post shuttle era?
- SO-6. How do changes in EPP affect the summer polar upper mesosphere, and what are the implications for PMCs?

2015 Extended Mission:

- SO-1. How does dynamical variability in the lower atmosphere couple to geospace weather? How do the fluxes of gravity waves at 50 km vary with latitude and season?
- SO-2. What governs the occurrence of mid-latitude PMCs?
- SO-3 What are the roles of solar and anthropogenic forcings on PMCs and the structure of the mesosphere?
- SO-4 Can the latitude variation of meteoric smoke be used to better understand the global mesospheric circulation?

2017 Extended Mission:

- SO-1. How does dynamical variability in the lower atmosphere couple to geospace weather? How do extraterrestrial phenomena propagate into the lower atmosphere?
- SO-2. What are the roles of solar and anthropogenic forcings on PMCs and the structure of the mesosphere?
- SO-3. What are the geographic and temporal distributions of mid-latitude PMCs and how are they influenced by waves and tides?

2020 Extended Mission:

- SO-1. What is the morphology of gravity waves entering the mesosphere and lower thermosphere?
- SO-2. How does planetary wave activity influence PMCs and composition in the mesosphere?
- SO-3. How does anthropogenic and extraterrestrial forcing impact the polar mesosphere?

2023 Extended Mission:

- SO-1. How does wave-induced coupling impact the MLT?
- SO-2. What drives decadal scale change in the MLT?

AIM has made steady progress on its science objectives, with the results often re-defining the state of knowledge in the field. A total of 377 AIM related journal articles have been published since launch in 2007, including 165 papers authored or co-authored by AIM team members.

2.2. Launch, Orbit, and Operations

2.2.1. Launch and Orbit

AIM was launched onboard a Pegasus XL rocket from Vandenberg Air Force Base on April 25, 2007 into a near circular (601 km apogee, 595 km perigee), 12:00 AM/PM sun-synchronous orbit. By 2017-18 orbital precession caused the β-angle (angle between the orbit plane and Earth - Sun vector) to pass through -90°, with a return to roughly -10° by mid-2020 (Figure 2.2.1). During this time, SOFIE measurements swept from polar through tropical latitudes, returning to polar latitudes in 2019. During parts of 2017-2018 the β-angle was sufficiently large (|β| > ~68°) that AIM was under nearly continuous solar illumination. CIPS benefited from this condition with nearly continuous global data collection, while SOFIE was unable to collet science data for several months because the sun did not rise or set as viewed from AIM. In spite of these interruptions, the SOFIE data collection periods provided new opportunities for science, as discussed below. SOFIE sunrise measurements were stopped on October 18, 2020 to conserve battery life during eclipse. During 2021 - 2024, the β-angle will be within ±30°, and SOFIE will have continuous polar coverage with normal PMC observations. During this time CIPS will continue operating with continuous imaging throughout the sunlit portion of the orbit, which will provide near-global latitude coverage. The enhanced CIPS capabilities also include concurrent GW/RAA and PMC measurements.

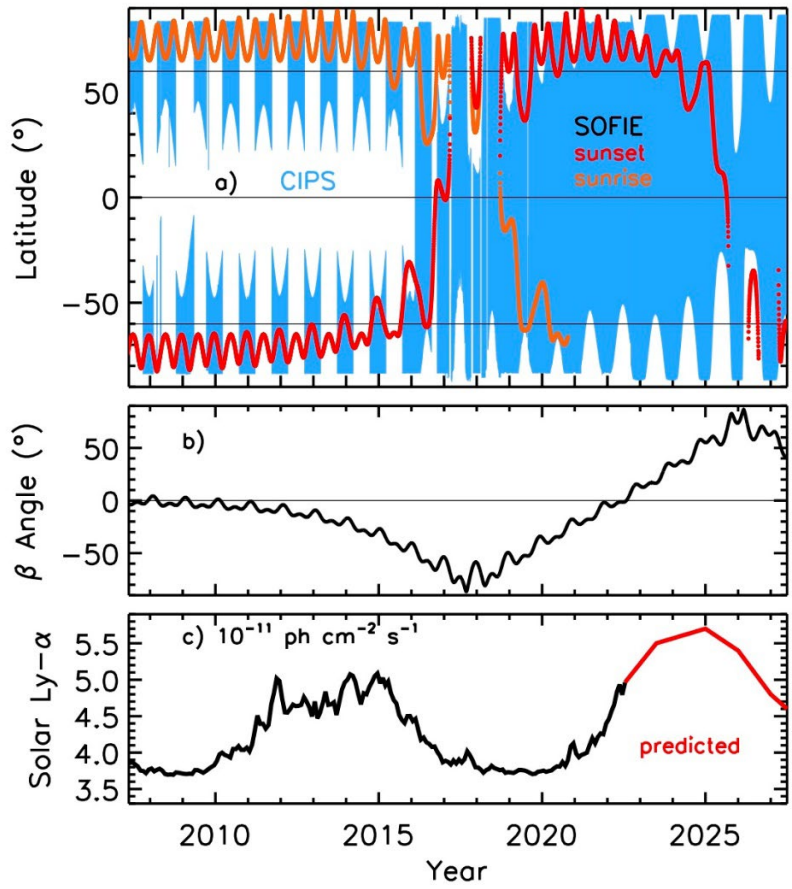

Figure 2.2.1. a) Latitude coverage of CIPS and SOFIE observations. b) AIM β angle. c) Solar Lyman-α, including a rough prediction.

2.2.2. Mission Operations Center (MOC)

Standard NASA services are used to connect the MOC to the primary ground stations located at Svalbard, Norway (SG1, SG2 and SG3), Poker Flat, Alaska (AS1 and AS3), North Pole, Alaska (USAK05) and Wallops Flight Facility in Virginia (WG1), as well as to the SN ground terminals at White Sands, NM. Three GN contacts and ~10 SN events per day provide for downlink of recorded telemetry and special command needs. The AIM MOC is fully automated so as to not miss any opportunities for command uplink should they occur. In addition, the AIM Project has obtained authorization from TDRSS management to use TDRSS to implement the AIM Scratchpad RTS capability, now built into the spacecraft autonomy, to upload custom command sequences and allow for future reconfigurations in the event command modulation lock should be lost again. Likewise, the MOC has been automated to send the necessary TDRSS Ground Control Message Requests to White Sands without the need for an operator in the event the scratchpad capability is needed again.

The AIM MOC has been instructed by NASA to move from the Closed to the Restricted IONet for future operations. In parallel to this activity, the MOC needs to upgrade from the current obsolescent Solaris system to a Linux based system to alleviate risk.

The AIM project will also need to certify on the new SN SGSS or the AIM usable TDRS's will be cut from five to one. In addition, the GCMR capability will need to be evaluated to determine if it is still compatible with AIM Morse coding needs. A backup concept for performing MC has been tested and would need to be integrated into the MOC in the event that GCMR's from SGSS do not meet the AIM requirements. It expected that this new capability would be adequate for performing routine MC operations, but would likely not be flexible enough to perform scratchpad operations if needed. In that event, the MOC will be limited to using TD-275 for such operations, which would increase the time needed for an uplink by five-fold.

The AIM project also needs to transition from the current Sybase database to Oracle to save funding over the long run. Oracle is provided by the university at no cost, but the Sybase database has an annual licensing fee. The cost of one year's license going forward would cover the full cost of making the transition, which would save money after the first year.

The AIM Flight Operations Team (FOT) is responsible for monitoring the status of the automated real-time operational contacts and performing post-pass analysis of the housekeeping data from the satellite bus and instruments. Plots are posted to the website after every contact for Flight Controller review, and are checked daily. In addition, undergraduate and graduate student Command Controllers assigned to subsystem teams check plots daily and provide Weekly Status Reports, Monthly Performance Reviews and Quarterly Long-term Trend Reports for their subsystems. The MOC produces Level 0 data products that are made available to instrument teams for higher level data processing. Routine science processing activities run unattended, with personnel regularly monitoring data processing activities and quality.

3. Science Instrumentation

The AIM experiment includes SOFIE, CIPS, and CDE (see Table 3). CDE experienced higher noise levels than expected on-orbit, triggering the need for new laboratory experiments, as well as the development of new data reduction approaches. The first eight months of CDE measurements were used to characterize the spatial and temporal variability of the cosmic dust

influx [*Poppe et al.*, 2011]. CDE noise levels continued to increase and after ~8 months the noise had reached an extent where the measurements were no longer usable. CDE was declared inoperable in early 2008, and deactivated in 2012. Because the CDE data were extremely challenging to analyze, as described below, the data were not made publicly available, as the few useful measurements are described in *Poppe et al.* [2011]. Recall that CDE was an exploratory instrument that cost roughly $1M, and was designed and built entirely by students. The shortfall in CDE results was mitigated using SOFIE observations, which in many ways exceeded the original CDE goals. SOFIE provided the first remote measurements of meteoric smoke in the mesosphere [*Hervig et al.*, 2009]. Since then SOFIE has been used to describe the seasonal variations in smoke, chemical composition of smoke, meteoric influx, and the meteoric smoke content of PMC particles [*Hervig et al.*, 2012, 2017a, 2017b, 2021, 2022].

Table 3. Summary of AIM instruments and key details.

Inst. Name	Remote or in situ sensing	Mass (kg)	Power (W), orbit average	Data Rate (Mbit / day)	PI	PI Organization	Inst. Status
CIPS	Remote	24	35	200	Cora Randall	LASP	OK
SOFIE	Remote	38	40	1000	Mark Hervig	GATS	OK
CDE	In situ	2	5	<1	Mihály Horányi	LASP	inoperable

3.1. The Cloud Imaging and Particle Size (CIPS) Experiment

CIPS is a nadir-imaging instrument that utilizes a four-camera design to discriminate the scattering of ultraviolet (UV) solar photons from PMC ice particles against Rayleigh scattering from the background sunlit atmosphere. The measurements of UV scattered radiation also enable measurements of gravity waves (GWs) near the stratopause. The CIPS instrument is described by *McClintock et al.* [2009], the PMC retrieval algorithm is described by *Lumpe et al.* [2013], and an introduction to the GW retrievals is given by *Randall et al.* [2017]. CIPS began routine measurements on May 24, 2007 and has operated flawlessly since that time. CIPS images of PMCs and GWs have a spatial resolution of 56 km^2. From 2007-2016, measurements of the PMC single scatter albedo were made over a range of scattering angles, thus providing a direct measurement of the PMC ice scattering phase function. This permitted retrievals of fundamental microphysical properties of the cloud particles, including albedo, particle radius and ice water content. More recent measurements have included fewer scattering angles, but more global coverage. Improved retrievals of the background Rayleigh scattering radiance have enabled robust determination of cloud albedo even without the phase function. In addition, these Rayleigh scattering retrievals have enabled the development of the Rayleigh Albedo Anomaly (RAA) data product, which is used to infer gravity waves near the stratopause.

3.1.1. CIPS Instrument Measurement Requirements

At launch the AIM measurement requirements were confined only to PMC measurements; the only GW requirement was to measure the signatures of GWs within the images of PMC albedo. There were no requirements to measure GWs near the stratopause, which was a capability that was developed later in the mission. Answering the first five original AIM mission science questions (Section 2.1) required panoramic images with global coverage for latitudes greater than 70°. In addition, measurements of cloud particle size distributions were required to address the first question and knowledge of GW morphology in the PMC region was required to address questions 2 and 3. This placed measurement requirements on the instrument, which were defined in terms of spatial resolution for the images and signal-to-noise ratio (*SNR*) for measuring directional albedo. Here we define directional albedo, $A(\chi)$, as the ratio of outgoing radiance observed at scattering angle (χ) to incident solar irradiance. The *SNR* requirements were defined in terms of albedo ratio (AR), which is the ratio of cloud directional albedo to the sum of cloud directional albedo plus Rayleigh-scattered directional albedo.

For PMC detection, the requirement is for a 2-sigma detection of clouds with $A=10^{-4}$ sr^{-1} in the common volume (CV) where the background is $A=10^{-5}$ sr^{-1} (AR=11). The CV is that region of the atmosphere located at a tangent altitude of approximately 83 km and extending approximately ±350 km on either side of the terminator along the line of sight from the spacecraft to the sun, where CIPS and SOFIE data overlap [*Gordley et al.*, 2009; *Russell et al.*, 2009]. The goal is for 2-sigma detection of clouds with $A=10^{-5}$ sr^{-1} against an $A=10^{-5}$ sr^{-1} background (AR=2). CIPS also views the sunlit atmosphere where background directional albedos may exceed 3×10^{-4} sr^{-1}. In this region, the albedo ratios are in the range $0.1<AR<2$. Spatial resolution of ~3 km is required to fully resolve the ~10 km minimum GW features (Fogle and Haurwitz, 1969). The CIPS performance requirements as defined for the prime mission, as well as the achieved performance, are given in Table 3.1-1 [*McClintock et al.*, 2009; Tables 1 and 3].

Table 3.1-1. CIPS performance requirements summary for prime mission.

Geophysical Parameter	**Instrument Requirement Instrument Performance**		
	Resolution (km)	**Accuracy**	**Precision (*SNR*)**
PMC Detection Limit	50 2.5	N/A N/A	*SNR* = 2 for AR* = 11 *SNR* = 19 for AR = 2
PMC Morphology	50 5	15% 12%	*SNR* = 20 for AR = 5 *SNR* = 38 for AR = 2
PMC Particle Size	200 5	50% 12%	*SNR* = 10 for AR = 5 *SNR* = 38 for AR = 2
Gravity Waves in PMCs	3 2.5	N/A N/A	*SNR* = 10 for AR = 11 *SNR* = 80 for AR = 11

*AR = albedo ratio = (cloud albedo+background albedo) / background albedo. Performance goals are enclosed in parentheses. *SNR* performance is for the achieved resolution in column 2.

As noted above, retrieval of atmospheric GWs near the stratopause was not an original AIM mission objective, so there were no measurement requirements imposed for stratopause GW

retrievals. Rather, the capability for retrieving GWs at the stratopause was developed as part of extended mission activities, for which the science objectives were written to be commensurate with the on-orbit measurement capabilities. These capabilities include the measurement of GWs at an altitude range of 50-55 km, for waves with vertical wavelengths longer than 15 km and horizontal wavelengths from 15-600 km, and with a horizontal resolution of 56 km^2.

3.1.2. CIPS Instrument Description

3.1.2.1. Instrument Overview

The CIPS instrument is described in detail by *McClintock et al.* [2009]. CIPS consists of four wide-angle cameras that cover a 120° (along orbit track) × 80° (cross orbit track) field of view (FOV). Figure 3.1.2.1-1 illustrates the instrument composite FOV projected onto the cloud deck near 83 km altitude, where it covers approximately 2200 km along track by 950 km cross-track. In this arrangement, the nadir cameras (PY and MY, for "plus" and "minus") maintain a nearly constant spatial resolution of better than 2.5 km across their entire FOVs, while spatial resolution of the sunward and anti-sunward (PX and MX) cameras varies from 2.5 km near nadir to 5 km in the extreme corners. During a data gathering sequence, the four cameras record simultaneous images to produce a single scene.

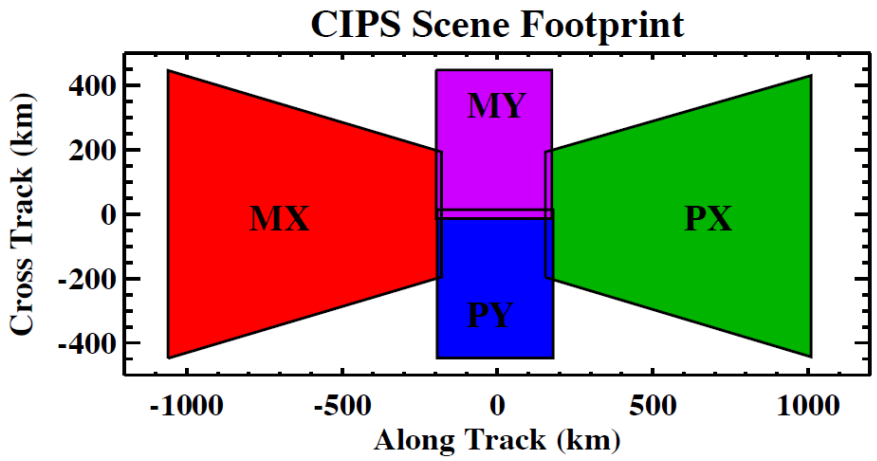

Figure 3.1.2.1-1. Relative alignment of the four CIPS cameras. The two "X" cameras point in the forward and aft direction, while the "Y" cameras have a primarily nadir orientation. The distance scales indicate the geometric footprint of a CIPS scene at the nominal PMC cloud deck altitude of 83 km. The PX camera always points in the sunward direction, which corresponds to the satellite ram (anti-ram) for Northern (Southern) Hemisphere measurements [*Lumpe et al.,* 2013].

In order to observe PMCs from orbit, the CIPS instrument spectral passband is designed to minimize the relative radiance contributions arising from sunlight reflected from the surface and scattered by the atmosphere. Absorption by ozone in the stratosphere and mesosphere results in a minimum in atmosphere plus surface radiance near 255 nm, the peak of the Hartley bands. We chose 265 nm for the center wavelength of the CIPS passband because that is the location of a

relative maximum in solar irradiance near the Hartley band peak. This results in the maximum PMC signal contrast relative to the Rayleigh-scattered background.

Figure 3.1.2.1-2 is an illustration of the assembled CIPS instrument. It consists of four wide-angle cameras, mounted on a nadir-facing platform, and the CIPS Processor Assembly (CPA). The CPA provides the instrument electrical interface to the AIM spacecraft as well as command and control for the individual cameras. These elements are mounted on a raised structure that provides the mechanical interface to the spacecraft. The cameras are equipped with one-time-actuated dust covers, which were opened approximately one month after launch. Custom light shades protect the optics from direct solar illumination and from sunlight scattered from illuminated spacecraft and instrument surfaces. Figure 3.1.2.1-3 shows an electrical block diagram for CIPS.

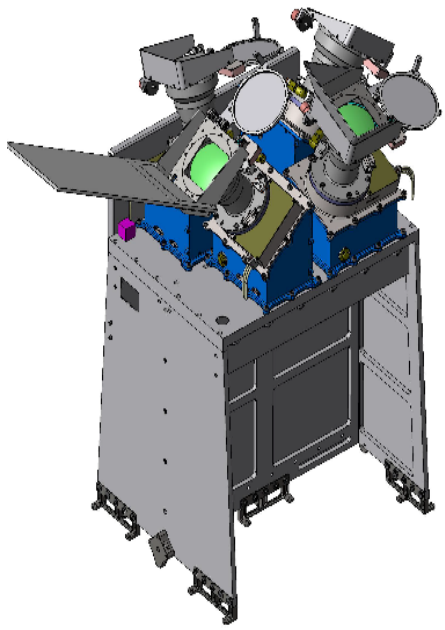

Figure 3.1.2.1-2. CIPS instrument configuration. *T*he computer-aided-design (CAD) drawing shows the cameras shown with their protective dust covers deployed. Custom optical shades on each of the cameras protect each camera from light scattered from outside its field of view. A long single-edge-baffle protects the sunward camera from direct solar illumination near sunrise and sunset. A pair of dual-output high voltage power supplies and the CIPS Processor Assembly are mounted beneath the instrument main optical bench that supports the four cameras.

Figure 3.1.2.1-4 shows the placement of CIPS on the AIM spacecraft before thermal blanket installation. The instrument is mounted on the earth-facing panel with its FOV aligned to the spacecraft Z-axis. For flight, thermal blankets cover the instrument except for the telescope apertures and radiators located in the direction of the spacecraft -Y and -X axes.

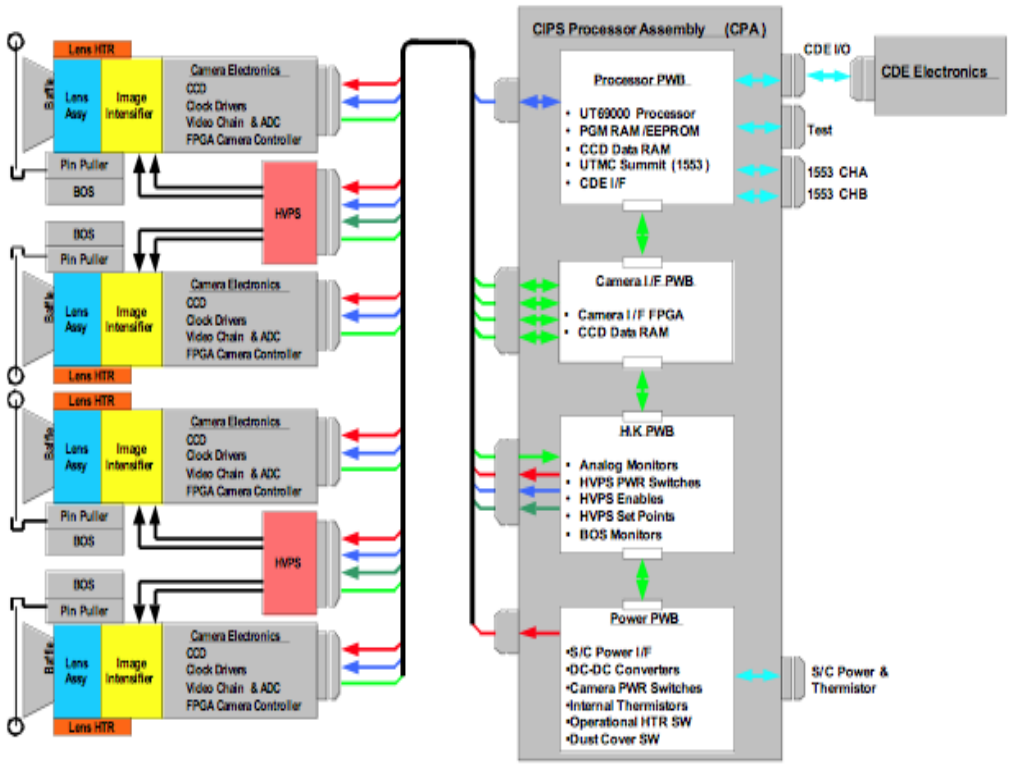

Figure 3.1.2.1-3. CIPS electrical block diagram. Red, blue, and green lines identify power, command, and data paths, respectively.

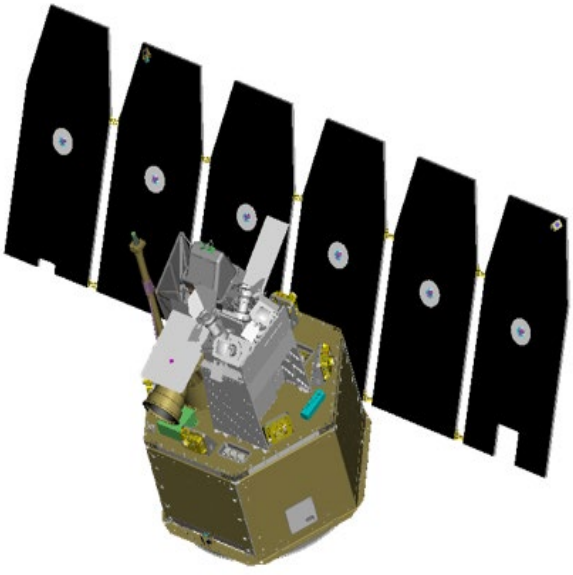

Figure 3.1.2.1-4. CIPS placement on the AIM spacecraft aligns the instrument FOV center with the spacecraft Z axis. For flight, thermal blankets cover the instrument except for the telescope apertures and radiators located in the direction of the spacecraft -Y and -X axes.

3.1.2.2. Camera Design and Optical Performance

Each of the four CIPS camera systems includes a lens assembly and interference filter, an image intensifier, and a CCD detector. The design is primarily driven by the requirements for ~ 3 km spatial resolution at nadir (imaging) and for 2-σ detection of clouds with $A=10^{-5}$ sr^{-1} against an $A=10^{-5}$ sr^{-1} background (radiometric sensitivity). Figure 3.1.2.2-1 shows the optical layout of a CIPS camera that consists of three fused silica lenses, four calcium fluoride (CaF_2) lenses, and three fused silica plates, which comprise the interference filter (two substrates) and the image intensifier window. It is a telecentric design with an effective focal length of 24.85 mm.

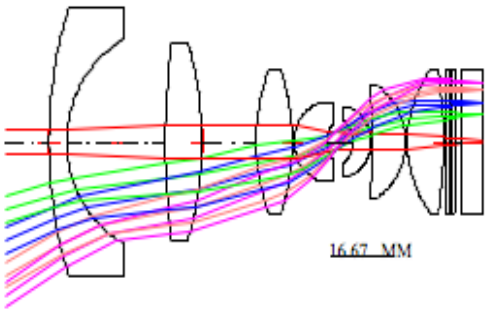

Figure 3.1.2.2-1. CIPS lens optical layout showing ray paths for 5 field points. The telecentric design insures that ray bundles exit the final lens parallel to the lens optic axis.

3.1.2.3. CIPS Detector Description

Sealed Hamamatsu V5180 image intensifiers are the ultraviolet detectors for the CIPS cameras. Each intensifier is equipped with a Cesium Telluride photocathode, deposited on the interior surface of a 6 mm thick fused silica input window, that converts ultraviolet photons with wavelengths near 265 nm to photoelectrons with a quantum efficiency of ~0.1. The photoelectrons are accelerated through a 40-volt potential and proximity-focused onto the input surface of a microchannel plate (MCP) where they are multiplied. Output electrons from the MCP are further accelerated into a P-43 phosphor by a 6-kilovolt potential producing a localized burst of visible photons (mean wavelength ~545 nm). Photons from the phosphor output are coupled through a fiber optic faceplate to the input of an Atmel TH7899M, full-frame CCD detector, where they are detected. During nominal operations voltage is continuously applied to the MCP and phosphor from a high voltage power supply (HVPS), while the voltage between photocathode and the MCP input is gated on during imaging and gated off during CCD readout, providing an electronic shutter.

3.1.2.4. CIPS Camera Mechanical Configuration

Figure 3.1.2.4-1 is an exploded view of a single camera, which consists of three major components. The first component is the camera base, which provides the enclosure for the detector and its three electronics boards and acts as the mechanical interface to the main instrument structure shown in Figure 3.1.2.1-2. Its top surface is machined with a 19˚ angle for the nadir cameras and a 39˚ angle for the fore and aft cameras to orient the boresight relative to the spacecraft control axes. In Figure 3.1.2.4-1 the top board of the detector assembly is separated from its housing to display the CCD chip, which has a fiber optic faceplate bonded to its input. The second camera component is the housing for the image intensifier. It is separate from the detector assembly

and contains the intensifier and an electrical filter board, which provides an interface between the intensifier and the HVPS that produces the voltage to operate the intensifier. A leaf spring assembly presses against the back of a CCD mounting plate and maintains contact between the output surface of the intensifier and the input surface of the CCD faceplate. The third camera component is the lens assembly. It is mounted to the intensifier housing and held in place by socket-cap screws and two stainless steel alignment pins. A spacer maintains the separation between the lens and intensifier housing and its thickness is adjusted during assembly to focus the system.

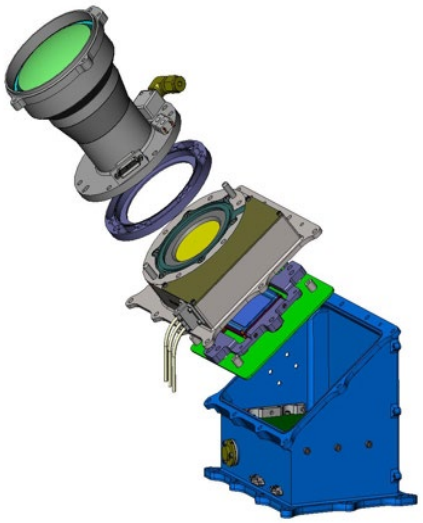

Figure 3.1.2.4-1. Exploded view of a single camera showing the detector housing, CCD electronics board, image intensifier housing, spacer, and lens assembly.

3.1.3. CIPS Instrument Observation Requirements and Capabilities.

Table 3.1.3 summarizes the key performance characteristics of the cameras [adapted from *McClintock et al.*, 2013; Table 2 therein].

Table 3.1.3. CIPS camera, detector, and instrument characteristics.	
Camera	
Effective focal length	24.8 mm
Focal ratio	F/4
Field of view	44° × 44°
Spectral passband	265±7.5 nm
Detector	
Configuration	Intensified CCD
Intensifier	Hamamatsu V5180U-03
Configuration	CsTe photocathode, 40 mm Dia
CCD	Atmel TH7899 (MPP)
Pixel size	0.014 mm
Imaging pixel format	2048 × 2048
Dark current	200 e^-/pixel/s @ 20°C; 40 e^-/pixel/s @ 0°C
Read noise	35 e^-
Pixel well depth	230,000 e^-
Amplifier gain	32 e^-/DN
Instrument	
Mass	21.8 kg
Orbit average power	34.5 W
Dimensions	38 × 33 × 64 cm^3

3.1.4. CIPS Data Acquisition

CIPS has operated with five different observing modes, the sampling for which is illustrated in Figure 3.1.4-1. The latitude range observed by CIPS is mode-dependent, which explains the shifts in latitude sampling shown above in Figure 3.1.4. From launch until 11 February 2016 the instrument operated in the Summer Pole mode. In this mode the CIPS scenes, which consist of 4-camera images with a 0.75-second exposure time, were acquired every 43 seconds only over the summer hemisphere mid to high latitudes. Here "summer" is defined as the time period from spring to fall equinox in the respective hemisphere. From 12 February 2016 until 23 February 2017, and from 22 November 2017 until 25 February 2018, CIPS operated in the Continuous Imaging Day + Night mode. In this mode, images were taken every three minutes throughout the orbit. This mode was designed to increase the latitude sampling in order to take

advantage of the CIPS gravity wave measurement capability. Even though pragmatic operational considerations dictated that CIPS images be acquired throughout the orbit, the night-side images cannot be used for science investigations. In 2017 from 24 February until 21 November, CIPS operated in the Continuous Imaging mode under Full Sun conditions. During these months roll control was implemented to maintain adequate pointing. Because of residual variations in the pointing, however, there were negative impacts on the calibration and retrievals of both PMCs and RAA. Therefore, at the current time, science data from 24 February to 21 November of 2017 have not been produced. During the second Full Sun period, from 26 February to 20 September of 2018, we successfully implemented stable nadir pointing. Thus, scientifically valid sunlit images were acquired throughout the orbit at a 3-minute cadence. In the fall of 2018 a new observing sequence, Continuous Imaging Dayside Only, was implemented in order to optimize image acquisition over the full range of sunlit latitudes. This observing mode began on 3 November 2018 and is currently operational.

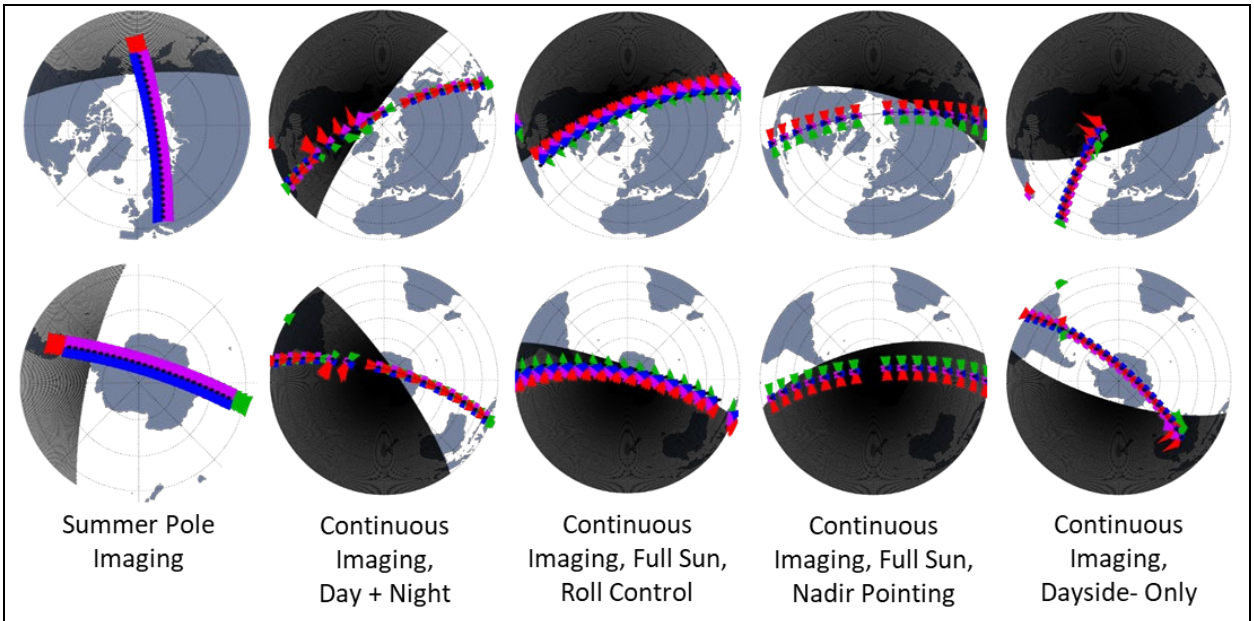

Figure 3.1.4-1. Examples of CIPS sampling geometry in the northern hemisphere (top) and southern hemisphere (bottom) for the five different observing modes. Camera colors are consistent with the color scheme in Figure 3.1.2.1-1.

3.2. The Solar Occultation for Ice Experiment (SOFIE)

SOFIE measures vertical profiles of limb path atmospheric transmission within 16 spectral bands between 0.29 and 5.32 μm wavelength (λ). Occultation measurements are accomplished by monitoring solar intensity as the satellite enters or exits the Earth's sunlit side (spacecraft sunrise or sunset, see Figure 3.2-1). The bands are used in pairs to form a channel, where one band measures the target gas (or aerosol) within a strongly absorbing spectral region with the other in a weak region (see Table 3.2-1). The electronic difference of the strong and weak bands is measured onboard, with the application of electronic gain ($G_{\Delta V}$). The difference signals eliminate (or greatly reduce) many common-mode instrumental error sources, in addition to some kinds of atmospheric interference. SOFIE measurements are used to retrieve the vertical profiles of temperature, five trace gases (O_3, H_2O, CO_2, CH_4, and NO), PMC extinction (at 9 wavelengths), and meteoric smoke extinction (at 3 wavelengths).

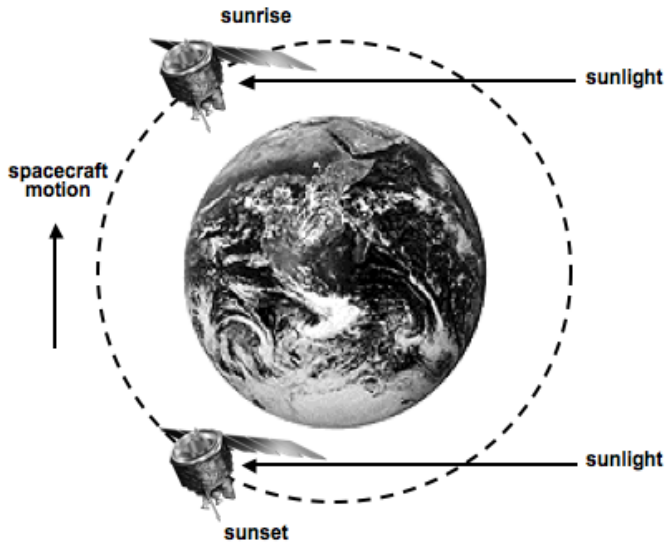

Figure 3.2-1. Solar occultation measurement geometry depicting solar rays passing through the limb of the Earth's atmosphere during spacecraft sunrise and sunset.

3.2.1. SOFIE Measurement Requirements and Capabilities

Each SOFIE channel consists of two broadband radiometer measurements (referred to as bands), one located in a wavelength region of strong absorption by the target species (V_S) and one in a spectrally adjacent region of weaker absorption (V_W). The spectral locations of each measurement were required to have sufficient absorption by the target species, and minimal interference from unwanted absorbers. The chosen bands have filter widths equal to or greater than 2%, and allow the mean absorption to be modeled with 0.5% uncertainty or less. Measurements of the difference signal ($\Delta V = (V_w - V_s)\ G_{\Delta V}$) are amplified by an electronic gain, $G_{\Delta V}$. Instrument performance can be summarized using the end-to-end-signal-to-noise ratio (S/N). Required S/N values were derived by considering the precision needed for the science retrievals (e.g. temperature or H_2O mixing ratio), with appropriate flow down through detailed models of the instrument and atmosphere. The pertinent SOFIE characteristics related to the 16 bands (8 channels) are given in Table 3.2-1. The SOFIE retrieval parameter altitude range and precision are summarized in table 3.2-2. Note that the achieved performance exceeds requirements in every case.

Table 3.2-1. SOFIE channel / bandpass characteristics.

Channel	Band	Target[1]	Center λ (μm)	Band Limits FWHM (cm^{-1})	$G_{\Delta V}$	Signal-to-noise
1	1	O_3 s	0.292	33650 - 34983	30	1.0×10^4
	2	O_3 w, p, m	0.330	29633 - 30990		1.0×10^4
2	3	PMC s, m	0.867	11324 - 11756	300	1.0×10^6
	4	PMC w, m	1.037	9439 - 9851		1.0×10^6
3	5	H_2O w, p	2.462	4020 - 4106	96	2.5×10^4
	6	H_2O s	2.618	3783 - 3858		2.5×10^4
4	7	CO_2 s	2.785	3555 - 3626	110	3.0×10^5
	8	CO_2 w, p	2.939	3369 - 3436		3.0×10^5
5	9	PMC s	3.064	3233 - 3295	120	1.0×10^5
	10	PMC w	3.186	3106 - 3172		1.0×10^5
6	11	CH_4 s, p	3.384	2922 - 2989	202	4.0×10^5
	12	CH_4 w, p	3.479	2846 - 2903		4.0×10^5
7	13	CO_2 s	4.324	2259 - 2370	110	4.0×10^5
	14	CO_2 w, p	4.646	2122 - 2183		4.0×10^5
8	15	NO w, p	5.006	1979 - 2017	300	3.0×10^5
	16	NO s	5.316	1853 - 1910		3.0×10^5

[1]s indicates strongly absorbing band, w denotes weakly absorbing band, p or m denotes PMC or meteor smoke measurement as a secondary target.

Table 3.2-2. SOFIE science parameter retrieval performance. Note that the achieved performance given here exceeds requirements in every case.

Retrieved Parameter	Altitude Range (km)	Precision at 83 km (unless otherwise noted)
Temperature	15 - 105	0.2 K
O_3	20 - 105	10 ppbv
H_2O	15 - 100	70 ppbv
CO_2	30 - 55	2 ppmv (30-55 km)
CH_4	15 - 79	5 ppbv (70 km)
NO	30 - 149	39 ppbv
PMC extinction	cloud	5×10^{-8} km^{-1}
Meteor Smoke extinction	35 - 85	2×10^{-8} km^{-1}

3.2.2. SOFIE Instrument Description

3.2.2.1. Optical Design

SOFIE uses a cassegrain telescope with a 10.16 cm entrance pupil. An elliptical primary mirror (16.76 × 11.55 cm) directs the incoming beam onto a focusing mirror and then to a secondary mirror (see Figure 3.2-2). The backside of the secondary mirror contains a pickoff mirror that directs a portion of the beam into the sun sensor module. The main beam passes through a field stop that determines the instantaneous (FOV) of 2.1 arcmin vertical × 5.6 arcmin horizontal. The beam is chopped at 1000 Hz using a tuning fork device, and directed into the channel separation module (CSM) where incoming energy is divided into the 16 spectral bands. A neutral density (ND) filter (transmission ranging from 0.398 in band 1 to 0.303 in band 16) is located at the CSM entrance to mitigate IR detector response nonlinearity by reducing optical throughput. Light terminates on the detector as an aperture image (i.e. pupil imaging system) to minimize the liability of signal drift due to coupling of solar image gradients with response gradients over the detector surface. This also insures a nearly identical matching of FOV for all detectors.

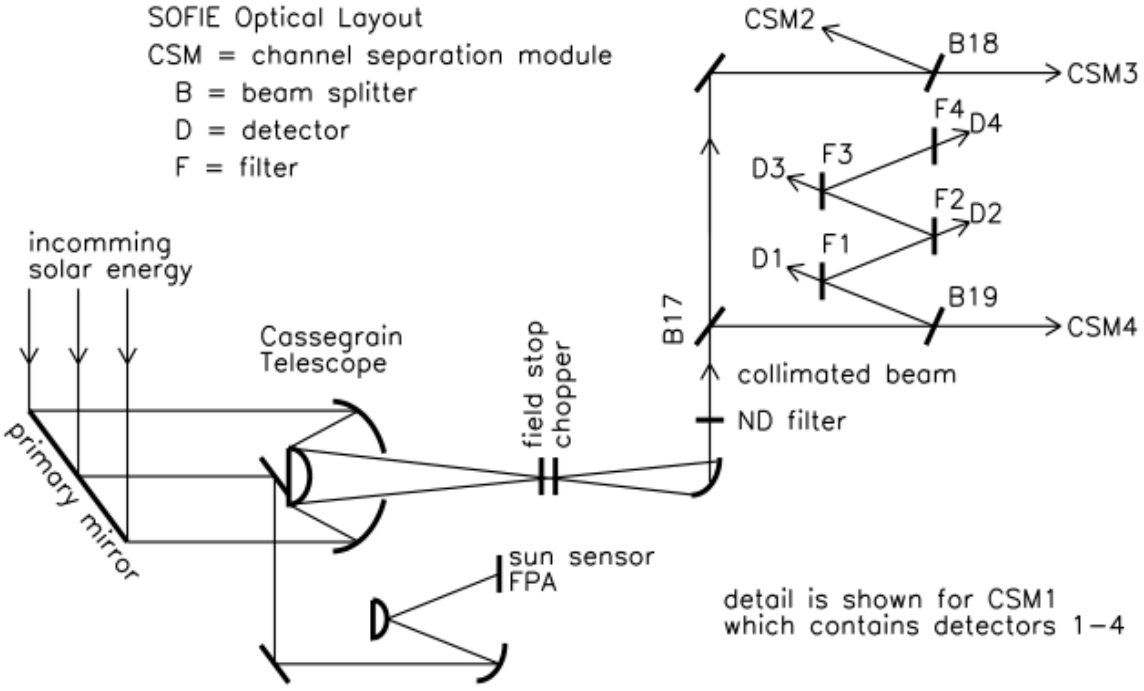

Figure 3.2-2. SOFIE optical system block diagram, showing the location of beam splitters, mirrors, and the four CSMs. Detail shown for CSM 1 includes the detectors and cascading filters.

Within the CSM, energy is divided into 16 spectral bands using a combination of dichroic beam splitters and bandpass filters (Figure 3.2-2). The CSM consists of four modules, each containing four bands that are close in wavelength. Spectral division within each CSM module is accomplished using cascading filters, which accept energy within the desired bandpass and reflect all other wavelengths to the next filter downstream. After the bandpass filter, the beam encounters a parabolic mirror which directs it onto the detector. All detectors are mounted on three-stage

thermo-electric coolers (TECs) and packaged within a vented housing that contains an anti-reflective window. Bands 1 and 2 use 1 mm square photo-voltaic (PV) silicon carbide detectors and bands 3 and 4 use 1 mm diameter circular PV germanium detectors. The silicon carbide detectors have a sharp response cutoff long-ward of 0.4 μm wavelength and thus are ideally suited for the channel 1 UV measurements. The IR bands (5-16) use 1 mm square photo-conductive (PC) HgCdTe (MCT) detectors (see Table 3.1-1), which were chosen for high signal-to-noise ratio and low implementation cost. The MCT detectors were found to have greater response nonlinearity than desired, but accurate calibration of nonlinearity was obtained in the lab over the complete measurement dynamic range. In addition, SOFIE science is predominantly acquired over a signal dynamic range of 2% or less (small variations on a large solar signal), and it was determined that system performance would be more than adequate for mission objectives.

3.2.2.2. Signal Conditioning Electronics

Three measurements are accomplished for each channel, the weak and strong band radiometer signals (V_w and V_s) and the difference of these signals (ΔV). The SOFIE analog signal path from detector to digitization is illustrated in Figure 3.2-3. Output signal from a detector preamp undergoes signal conditioning including synchronous rectification at 1000 Hz. The weak and strong band signals have adjustable attenuators which can induce gains (G_W and G_S, respectively) from 0 to 1 as commanded using a 12-bit controller. The radiometer and difference signals are digitized using a 14 bit analog to digital converter (ADC) operating from -3 to 3 V. The signals are oversampled (32 times during 50 ms) and used to determine statistical 16 bit values (91.6 μV / count) that are reported at 20 Hz (every 50 ms). Due to the sampling sequence, a given signal can be offset from the start of a 20 Hz cycle by up to 37.5 ms, and these offsets are removed during ground signal processing. The radiometer signals are digitized between 0 and 2^{15} counts (0 to 3V) providing a granularity in measured transmission of 3.05×10^{-5}. The ΔV measurements operate from -2^{15} to 2^{15} counts providing a transmission grannularity ranging from 1.02×10^{-6} for $G_{\Delta V} = 30$ to 1.02×10^{-7} for $G_{\Delta V} = 300$.

The ΔV signals are balanced in orbit to a desired exoatmospheric value, ΔV_{bal}, using the strong and/or weak band attenuators. ΔV_{bal} is set before the sun is encountered based on measurements from previous events. The value of ΔV_{bal} is flexible, with the greatest dynamic range realized for $\Delta V_{bal} = -3$V. The ΔV balance precision is a function of the balance attenuator step size and the ΔV gain. The 12-bit attenuators give ΔV balance precision ranging from 120 counts for $G_{\Delta V} = 30$ and 1200 counts for $G_{\Delta V} = 300$. In ground processing $G_{\Delta V}$ is removed from the ΔV measurements which are then mathematically adjusted to be consistent with $\Delta V_{bal} = 0$. Thus, a precise ΔV balance condition in-orbit is unnecessary.

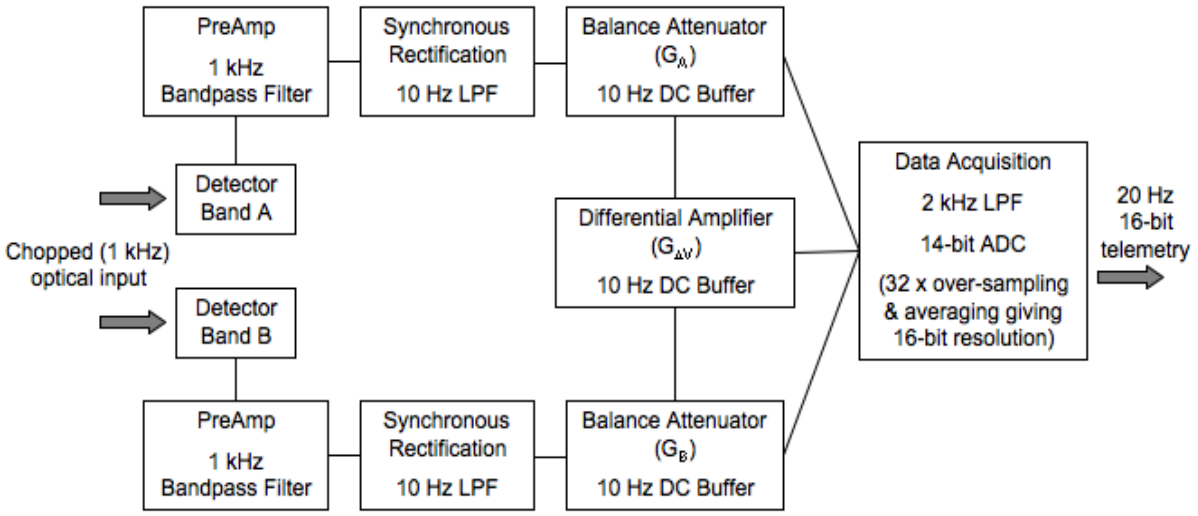

Figure 3.2-3. Electrical block diagram for a pair of SOFIE detectors comprising a single channel. The two paths represent the strong and weak band signal chains (LPF denotes low pass filter and ADC denotes analog to digital converter).

3.2.2.3. Sun Sensor

The SOFIE instrument contains a sun sensor used to determine the angular location of the solar image relative to the science FOV. Given orbital ephemeris information and FOV location relative to the sun, tangent altitude can be accurately determined, and tangent altitude spacing between measurement samples can be determined with extreme accuracy. SOFIE pointing is controlled by the spacecraft, and spacecraft pointing offsets are refined using sun sensor information. Solar image location is important because intensity varies across the solar disk and movement of the FOV can change the underlying source intensity (V_0), which must be known to infer atmospheric transmission. Given knowledge of the solar intensity distribution from exoatmospheric solar scans (which are in terms of sun sensor angles), the exact FOV location is unimportant if relative movement of the FOV on the solar disc can be determined precisely. Thus, SOFIE requires pointing knowledge precision rather than absolute accuracy.

The sun sensor intercepts a portion of the incoming solar beam immediately after the primary mirror (Figure 3.2-2). This beam is directed through a neutral density filter to reduce intensity and a spectral bandpass filter with a center wavelength of 701.4 nm and 23 nm width. The sun is imaged onto a radiation hardened CMOS focal plane array (FPA) comprised of 1024 x1024 pixels. FPA signals are acquired in rectangular sub-regions and pixel intensities are digitized using a 10-bit converter. The sun sensor FPA field of view of 2.04° in azimuth and 2.025° in elevation easily encompasses the 0.5° diameter solar image (Figure 3.2-4). Individual FPA pixels have 15 μm pitch which subtends ~7.10 arcsec in azimuth and ~7.18 arcsec in elevation at the center of the array. The effective pixel resolution is about 17 arc seconds due to light dispersion by the sun sensor optics. This blur actually increases the precision in determining movement of the solar image edge on the FPA.

The sun sensor determines solar position by first locating the solar image on the FPA using a 2-D center of mass algorithm (coarse tracking), and then precisely detecting the solar top, bottom, left, and right edge locations (fine tracking). The edge detection routine uses a small region of interest (ROI) at each of the four edges, which are 15 pixels across the edge by 21 pixels parallel to the edge (Figure 3.2-4). Each row of pixels in the top and bottom ROI are averaged (i.e. parallel to the edge) to produce a pixel intensity profile across the edge. The edge is defined by the position of a relative intensity value, I_E, nominally 25% of the brightest pixel average, and located in the on-board algorithm using linear interpolation on the two points surrounding I_E. Using pixel intensity averaging and linear interpolation reduces measurement noise and reduces sensitivity to erroneous results. Laboratory calibration indicated that the solar image edge location is determined with better than 0.7 arcsec precision in azimuth and elevation. This result confirmed theoretical predictions of the sun sensor performance capabilities which suggested a precision of less than 1 arcsec. In addition, PMC attenuation at the sun sensor wavelength is minor and does not affect tracking performance. The row sums are recorded and included in the telemetry stream at 20 Hz for subsequent analysis during ground processing. Initial results using enhanced edge modeling in ground processing have shown a precision of 0.2 arcsec or better. Ground analysis, that will include transmissions measured by the sun sensor, is expected to reduce the edge detection precision to under 0.1 arcsec.

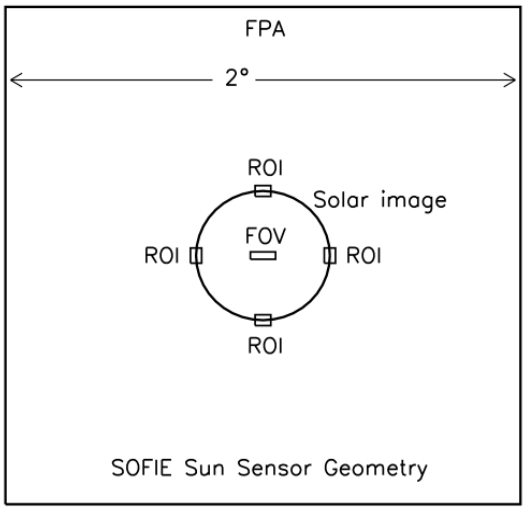

Figure 3.2-4. Dimensions of the SOFIE sun sensor focal plane array (FPA), solar image, and science FOV. Pixel regions of interest (ROIs) used to determine four solar edge locations are also shown. All dimensions are to scale, except the ROIs which are magnified by 50% for clarity.

3.2.3. SOFIE Instrument, Observation Requirements and Capabilities

SOFIE measures solar intensity as rays pass through Earth's atmosphere on tangent paths. These observations are required at altitudes from the Earth's surface (0 km) to 180 km altitude, at a vertical spacing of 1.5 km. The on-orbit vertical spacing is ~145 m (~10 times oversampled), which is a result of the detector readout cadence (20 Hz) and solar sink rate (~2.9 km s^{-1}). Table 3.2-3 summarizes the optical, physical, and electrical characteristics of the SOFIE instrument. SOFIE capabilities meet or exceed requirements, and have not changed since launch.

Table 3.2-3. SOFIE optical, physical, and electrical characteristics.	
Item	**Description**
Telescope Aperture Diameter	10.16 cm
Obscuration Diameter	3.0 cm
Entrance Pupil Area (A)	74.005 cm^2
Entrance Pupil Solid Angle (Ω)	9.139 x 10^{-7} sr
AΩ	6.763 x 10^{-5} cm^2 sr
Chopping Frequency	1000 Hz
Modulation Form Factor (Chopping)	0.406
Radiometric Electrical Noise Bandwidth	3.14 Hz
Radiometric Electrical Signal Bandwidth	2 Hz
Detector Analog Signal Digitization	14 bits, -3 to 3 V (co-added to give 16 bits)
Detector Signal Reporting Frequency	20 Hz
Sun Sensor Data Reporting Frequency	20 Hz
Sun Sensor Wavelength	701.4 nm (23 nm bandwidth)
Sun Sensor Field of View	2° x 2°
Radiometer Field of View (16-band average)	1.95 x 5.30 arcmin vertical x horizontal
Radiometer FOV location on Sun Sensor FPA	Elevation: 636.16 pixels Azimuth: 501.75 pixels

3.2.4. SOFIE Data Acquisition

SOFIE measures 24 science signals (16 radiometers and 8 difference signals, e.g. Table 3.2-1), at 20 Hz with multiplexing through 4 analog-to-digital converters (ADCs). The sun sensor sub-system reports the location of four solar edges, and the solar intensity at sun center (see section 3.2.2.3 for detail), also at 20 Hz. SOFIE housekeeping measurements include numerous temperatures, and voltages (or currents) for critical components (TECs, chopper, detectors), as described in detail on the SOFIE webpage (sofie.gats-inc.com). The SOFIE science, sun sensor, and housekeeping data are transmitted directly to the spacecraft on a continual basis (SOFIE has no internal data storage). The spacecraft stores SOFIE data until it encounters contact with a ground (or orbiting) receiving station.

3.3. Cosmic Dust Experiment (CDE)

CDE is a polyvinylidene fluoride (PVDF) based impact cosmic dust (i.e., meteoroid) detector, and is nearly identical to the Student Dust Counter (SDC) onboard the New Horizons mission to Pluto [*Horányi*, 2008; *Poppe et al*., 2010]. PVDF detectors have been previously flown on several spacecraft, including the Cassini mission to Saturn [*Srama et al*., 2004], the ARGOS mission around Earth [*Tuzzolino et al.*, 2001a] and the STARDUST mission to comet 81P/Wild [*Tuzzolino et al.*, 2004]. PVDF is known to be mechanically and thermally stable, radiation resistant and non-responsive to energetic particle impacts, providing an ideal method for dust detection. CDE experienced higher noise levels than expected on-orbit, and after ~8 months the noise had reached an extent where the measurements were no longer usable. CDE was declared inoperable in early 2008, and deactivated in 2012. CDE science results were reported in *Poppe et al.*, [2011].

A number of techniques have been used to measure the cosmic dust influx into our atmosphere, including high-powered large- array (HPLA) radars [*Mathews et al*., 2001; *Janches and ReVelle*, 2005; *Sparks and Janches*, 2009], optical observations [*Horz et al.*, 1975; *Leinert*, 1975] and in situ dust detectors [*Love and Brownlee,* 1993; *Tuzzolino et al.*, 2001a; *Schwanenthal*, 2004]. HPLA radar offers a unique window on micron-sized dust flux measurements by analyzing the meteor head echoes generated by dust particles undergoing ablation in Earth's upper atmosphere. Recent work has attempted to refine the physical description of ablating particles and their detection via radar [*Fentzke and Janches*, 2008], yet such measurements are by nature limited to observations at specific terrestrial latitudes. In situ dust detectors, such as the Long Duration Exposure Facility (LDEF) [*Love and Brownlee*, 1993] and the Space Dust (SPADUS) instrument aboard the ARGOS spacecraft [*Tuzzolino et al.*, 2001a], have measured the terrestrial cosmic dust influx; however, significant uncertainty remains in the spatial and size distributions and variability thereof (Figure 3.3-1). The estimates for the flux of particles of < 10 μm in radius show disagreement on an order of magnitude, highlighting the difficulties of measuring the sub-millimeter dust flux.

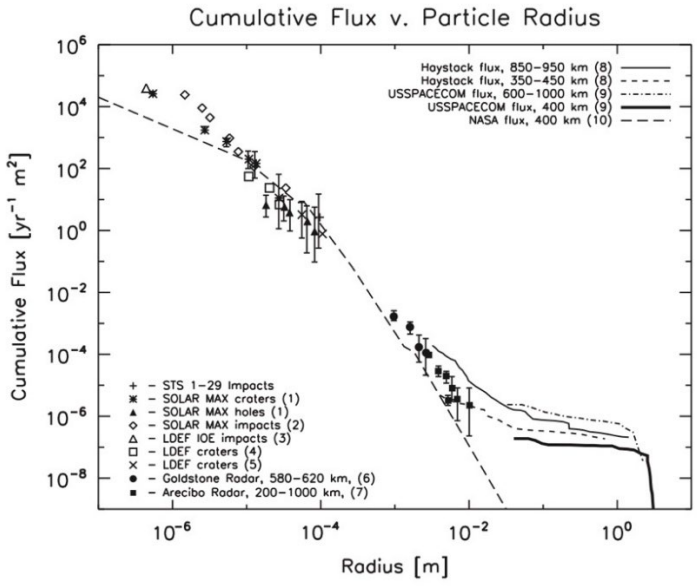

Figure 3.3-1. Cumulative flux versus radius for terrestrial cosmic dust from a variety of measurements. Adapted from *Gleghorn et al.* [1995]. References in the legend: (1) NASA/JSC; (2) *Laurance and Brownlee* [1986]; (3) *Simon et al*.; (4) *Bernhard et al.*; (5) *Humes*; (6) *Goldstein and Randolph* [1992]; (7) *Thompson et al.* [1992]; (8) *Stansbery et al.* [1995].

3.3.1. CDE Instrument Measurement Capabilities

CDE measurement characteristics and capabilities are summarized in Table 3.3.1.

Table 3.3.1. CDE measurement characteristics and capabilities.

Parameter	Capability
Time resolution of dust counts	1 s
Precision	10%
Detector Surface Area	0.11 m^2
Dust Size Range	1.5 μm < radii < 8 μm
Dust Mass Resolution	factor of 2 for 10^{-11} < m < $5x10^{-9}$ g
Altitude	Spacecraft altitude
Temporal Resolution (of final product)	1 week

3.3.2. CDE Instrument Description

Similar to the Student Dust Counter, CDE consists of 14, 28 μm thick PVDF detectors coated with 100 nm of aluminum–nickel and mounted to an external panel facing the zenith direction. Twelve of the detectors are exposed to space (referred to as the 'science' detectors), while two detectors are covered by aluminum cases and mounted to the underside of the instrument panel in order to detect background signals ('reference' detectors). When a dust particle impacts a detector, the AlNi layer is punctured and a crater is formed in the polarized PVDF, generating a fringing electric field around the crater [*Poppe et al.*, 2010]. This fringing electric field causes a change in the charge density on the AlNi plate, which is measured by an accompanying electronics box mounted to the inside of the AIM spacecraft. PVDF sensors are known to be susceptible to generating spurious signals, due to their piezo- and pyroelectric properties [*Nalwa*, 1995]. For this reason, as in the case of SDC, we use the two underside-mounted detectors as noise-monitoring channels. The measured event rate on the science detectors is due to dust impacts and noise, while the rate on the reference detectors is due to noise only. The final dust flux is calculated by subtracting the reference event rate from the science event rate and normalizing by observation time and instrument area. The instrument is divided into three sections: the detector, the front-end analog electronics, and the digital interface electronics, as described below.

3.3.2.1. Detector

The CDE detection principle is based on the depolarization signal a dust particle generates by penetrating a permanently polarized thin PVDF film [*Simpson and Tuzzolino*, 1985; *Tuzzolino*, 1992] Dust grains penetrating the thin film remove dipoles along their trajectory producing a fast electric charge pulse without requiring bias voltages. The produced signal is a function of particle mass and velocity. The physical construction of the detector is shown below. The PVDF film is mounted on a G4 board with a conductive adhesive connecting the positive electrode of the film to the top copper carrier. The second electrode is connected to the opposite copper carrier and ultimately to an electrical ground, Figure 3.3-2. The detector has an active area of 91.6 cm^2 and a

capacitance of 34.8nf. A suite of nine detectors provides us a total area of 824.5 cm^2. The detector suite will be mounted on an aluminum back plate, Figure 3.3-3. The overall volume of CDE will be 4800 cm^3 not including the volume encompassed by the structure that the CDE rests upon). Initial thermal analysis shows that this configuration has better heat dissipation characteristics than PVDF detectors used previously. The PVDF film is available from Measurement Specialties.

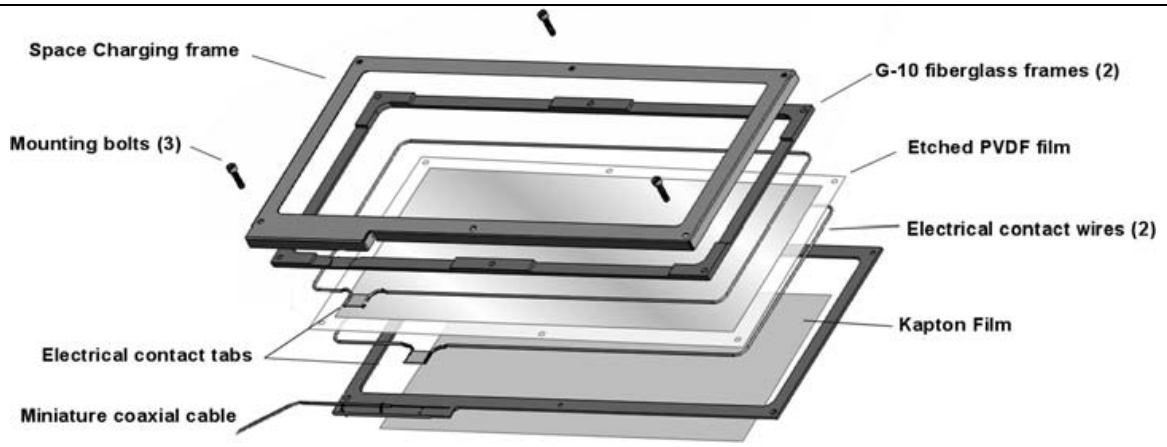

Figure 3.3-2. CDE elements, including an exploded view of a single S PVDF detector. The detector is mechanically bonded with structural epoxy. Electrical connection from the PVDF metalization to the signal wires is through silver-filled epoxy. The signal wires are soldered to miniature coaxial cables leading to the system electronics.

3.3.2.2. Front End Analog Electronics

The front-end electronics consist of an analog preamplifier and a shaping circuit. Each detector requires its own preamplifier and shaping circuit that will be located directly below the detector. The preamplifier is charge sensitive (AMP TEK A250) with the ability to use an external field effect transistor (FET). An external FET allows us to match detector capacitance with the FET thereby optimizing the A250 for use with our detector. The dual channel IF3602 manufactured by InterFET Corporation will serve as the external FET. The A250 was developed for aerospace, nuclear physics, nuclear monitoring, particle, gamma, and x-ray imaging.

The shaping circuit is a band-pass circuit with corner frequency set to the point where the noise in the circuit is at a minimum. This can be represented by $\tau_{shaper} = E_n * C_{Detector} / I_n$. A four stage nonlinear shaping circuit is used to allow the detection of more divisions for smaller particles than larger ones. After signal shaping, the pulse height detector (AMP TEK PH300) will hold the signal and alert the digital interface. The PH300 was developed for Aerospace, nuclear monitoring, particle, gamma, and x-ray imaging.

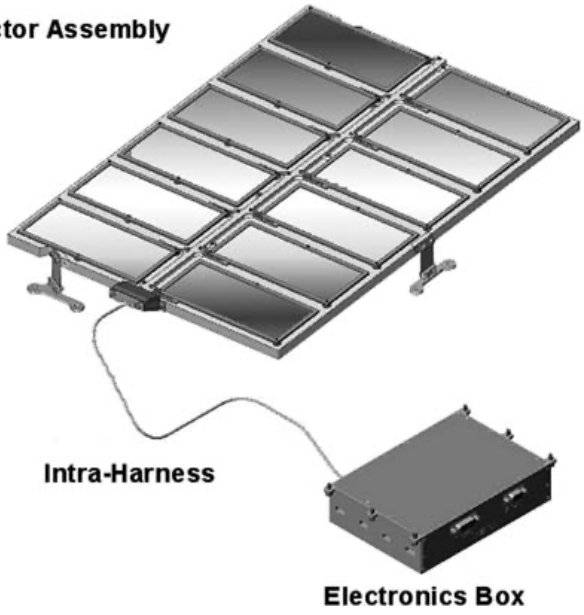

Figure 3.3-3. CDE PVDF detector layout. It weighs 1.6 kg and consumes ~5 watts of average power.

3.3.2.3. Digital Interface Electronics

The digital interface electronics provide the interface between the spacecraft C&DH system and the CDE. Each of the nine analog signals from the peak hold detectors are digitized and sent to the 54SX FPGA. The FPGA records event time, patch location, and signal amplitude. The 54SX signals the spacecraft computer and forwards the data over an RS422 interface. The majority of FPGA logic designs have significant heritage on two previous programs, Cassini and EOS Source. In both of these cases, data were integrated and binned in a similar manner to the dust detector data.

3.3.2.4. Software

All of the CDE functionality is contained in the FPGA, so that the instrument does not contain actual flight software. When CDE is turned on it immediately starts taking science data. Ground commands are required only to perform calibrations or reconfigure settings. The ground can also turn channels off or on, erase the flash memory, and request telemetry packets. 3.3.3. CDE Data Acquisition.

3.3.3. CDE Instrument Observation Requirements and Capabilities

CDE is accommodated on the space facing deck of the spacecraft and continuously monitors the influx of interplanetary dust particles (IDP). The instrument provides ~0.1 m^2 of sensitive area. It was designed to measure the mass of IDPs in the range of 10^{-12} to 10^{-9} g. It continues registering the impacts of bigger dust particles without the ability to determine their mass.

3.3.4. CDE Data Acquisition

CDE data are routed through the CIPS instrument CD&H electronics, where they are inserted into the CIPS data stream for telemetry. CDE provides several data packet types including science data, housekeeping information, calibration results, memory dumps, and message logs.

4. Data Products

This section describes the data products from the instruments on AIM along with a brief summary of the current distribution of that data. The AIM mission's instruments and status may be found in Table 3-1. Data levels are adapted from the EOS Handbook. The data levels are supplemented with additional product content classes for products that are not easily classified by the data level scheme. Below is a table describing the broad definition of the data level classifications. The description of how each instrument applies these definitions to their specific data is detailed in the instrument specific subsections.

Table 4-1. Summary of AIM instruments.

Inst. Name	Parameters Measured	Instrument Type	Inst. Status
CIPS	Scattered sunlight at 265 nm wavelength.	Four camera imager	OK
SOFIE	Solar intensity versus altitude, in 16 spectral bands, and the difference of band pairs.	Solar occultation	OK
CDE	Cosmic dust impacts.	In situ	Inoperable

Table 4-2. General data level definitions.

Data Level	Data Format	Brief Description	Source
Raw telemetry	CCSDS Transfer Frames	Raw telemetry	MOC
Level 0	CCSDS Packets, Resides in the MOC database.	Unprocessed instrument data at full resolution that has been separated by instrument or subsystem – time ordered with duplication removed	MOC
Level 1	NetCDF	Instrument data at full resolution, time-referenced and annotated with ancillary information including geometric parameters, that has been processed to radiometric / scientific units	SDC
Level 2	NetCDF	Derived geophysical parameters at the retrieval resolution	SDC
Level 3	NetCDF	Parameters mapped on a uniform, earth-referenced, space-time grid	SDC

4.1. CIPS Science Data Products

This subsection details the science data products produced by the CIPS instrument. Data for release and archiving is principally stored in the NetCDF format with higher level summary files in an appropriate format: text, png for images, and mp4 for movies.

4.1.1. CIPS Data Products Functional Description

CIPS data products fall into three categories: Level 0 and level 1 calibration and geolocation data, levels 2 and 3 PMC retrievals, and levels 2 and 3 Rayleigh Albedo Anomaly (RAA) retrievals.

Table 4.1-1. CIPS data level definitions

Data Level	Data Format	Brief Description	Source
Level 0	CCSDS Packets	Raw, uncalibrated images, binned on-chip to 170 × 340 pixels. Common to PMC and RAA retrievals.	CIPS Science Data Center (CSDC)
Level 1a	NetCDF	Calibrated and geolocated albedo. Files contain all images from a single camera over one orbit, so there are 4 files per orbit (one per camera). Common to both PMC and RAA retrievals.	CSDC
Level 1b PMC-only	NetCDF	Map-projected albedo at 25 km^2 resolution, calculated from level 1a data. One NetCDF file per orbit. These files register all measurements of a single location into data "stacks" to facilitate level 2 retrievals. Used only for PMC retrievals, v4.20 and earlier versions.	CSDC
Level 1p	NetCDF	Map-projected albedo at 56.25 km^2 resolution, calculated from level 1a data. One NetCDF file per orbit. This is used to create level 2 files for v5 and later PMC retrievals, and for all RAA retrievals	CSDC
Level 2 PMC-only	NetCDF and png	Retrieved cloud parameters at 25 km^2 resolution for v4 and earlier versions, and at 56.25 km^2 resolution for v5 and later versions. Four files per orbit containing, respectively: (1) geolocation data; (2) cloud properties, including albedo, particle radius, and ice water content; (3) cloud phase function (cloud albedo vs. scattering angle); (4) retrieved ozone parameters. Cloud albedo in file #2 is normalized to 90° scattering angle and nadir view.	CSDC
Level 3a PMC-only	NetCDF and png	Daily cloud albedo maps, produced by combining level 2 data from all individual orbits on a given day. Same resolution as level 2.	CSDC

Level 3b PMC-only	mp4	Movies of daily cloud albedo maps for an entire PMC season. 5×5 km resolution for v4 and earlier; 7.5×7.5 km resolution for v5 and later.	CSDC
Level 3c PMC-only	IDLsave and ascii (v4 and earlier); IDLsave and NetCDF (v5 and later)	Season-long files of level 2 data. Retrievals of cloud albedo, particle size, and ice water content from each orbit are binned in one-degree latitude bins and output for an entire PMC season.	CSDC
Level 3d PMC-only	ascii	Season-long files of level 2 data in the "common volume" (CV) viewed by both CIPS and SOFIE. The CIPS Level 3d data are pulled directly from the Level 2 data files, and consist of the subset of pixels that are co-located with the SOFIE line-of-sight (LOS). The CIPS level 3d file contains the primary CIPS level 2 retrieval products and associated auxiliary data, in the CV, for each orbit over an entire PMC season.	CSDC
Level 3e PMC-only	ascii	Like Level 3d, but these files contain data that are coincident with a selected group of ground stations.	CSDC
Level 2a RAA-only	NetCDF and png	Retrieved CIPS RAA data in a scene-by-scene format. A CIPS scene contains simultaneous images from the four CIPS cameras. Four files per scene: (1) geolocation, (2) measurement geometry, (3) RAA, (4) FFT filtered RAA plus RAA variance.	CSDC
Level 2b RAA-only	NetCDF and png	Retrieved RAA and RAA variance in an orbit-by-orbit format. All the scenes from an orbit are merged together by combining overlapping pixels from different cameras in much the same way as the CIPS Level 2 PMC data products.	CSDC
Level 2c RAA-only	png	Global maps of RAA and RAA variance, made by superimposing level 2b data for 1-5 days. For qualitative purposed only.	CSDC
Level 3a RAA-only	NetCDF and png	Global maps of gridded (1°x1°) RAA variance data.	CSDC

4.1.2. CIPS Science Data Distribution

The CIPS Data Center includes personnel and facilities for processing all CIPS data through the retrieved and value-added data products, and for producing CIPS data for distribution and archival. Data for levels 2 and higher are disseminated to the community via the CIPS webpage (http://lasp.colorado.edu/aim/). CIPS data are also available on NASA's Space Physics Data Facility (SPDF), under the Heliophysics Data Portal (HDP). The SPDF CIPS interface includes all data from Levels 1 through 3, in addition to documentation and software.

4.2. SOFIE Science Data Products

SOFIE science data products fall into two categories: primary science retrievals (level 2 products, Table 4.2-1), and secondary science retrievals (level 4). The L4 products include detailed physical characteristics of PMC particles, as summarized in Table 4.2-2. L4 results are retrieved from the reported L2 products, and are reported in one file for each PMC season (i.e., polar summer).

Table 4.2-1. SOFIE L2 science data products.

Product	Altitudes	Source Measurement (Wavelength)
Temperature	10 -102 km	band 13 (4.324 μm) & refraction (0.701 μm)
H_2O	17 - 95 km	band 6 (2.618 μm)
O_3	20 - 105 km	band 1 (0.291 μm)
CH_4	21 - 80 km	band 11 (3.384 μm)
NO	35 - 149 km	band 16 (5.316 μm)
CO_2	30 - 55	band 13 (4.324 μm)
0.330 μm Aerosol Extinction	17 - 95 km	band 2 (0.330 μm)
0.867 μm Aerosol Extinction	17 - 95 km	band 3 (0.867 μm)
1.037 μm Aerosol Extinction	17 - 95 km	band 4 (1.037 μm)
0.867 - 1.037 μm Aerosol Extinction Difference	41 - 95 km	channel 2 (band 3 minus band 4)
2.462 μm Aerosol Extinction	17 - 95 km	band 5 (2.462 μm)
2.939 μm Aerosol Extinction	17 - 95 km	band 8 (2.939 μm)
3.064 μm Aerosol Extinction	17 - 95 km	band 9 (3.064 μm)
3.186 μm Aerosol Extinction	17 - 95 km	band 10 (3.186 μm)
3.479 μm Aerosol Extinction	17 - 95 km	band 12 (3.479 μm)
4.646 μm Aerosol Extinction	17 - 95 km	band 14 (4.646 μm)
5.006 μm Aerosol Extinction	17 - 95 km	band 15 (5.006 μm)

Table 4.2-2. SOFIE L4 science data products. The results are retrieved from the various PMC extinctions, and are reported only at PMC heights (~80-90 km).

Product	Source PMC Extinctions
Ice layer top altitude (km)	band 9
Ice layer peak altitude (Z_{max}) (km)	band 9
Ice layer bottom altitude (km)	band 9
Ice volume density ($\mu m^3\ cm^{-3}$)	band 9
Ice mass density ($g\ km^{-3}$)	band 9
Axial ratio of oblate & prolate spheroids	bands 8, 9, & 10
Ice temperature, ice-T (K)	bands 8, 9, & 10
Axial ratio of oblate spheroid, retrieved simultaneously w/ ice-T	bands 8, 9, & 10

Gaussian size distribution parameters (assuming pure ice): concentration (cm^{-3}), median radius (nm), width (nm)	chan. 2 difference & band 9
Effective radius (nm)	chan. 2 difference & band 9
Volume fraction of meteoric smoke in ice	chan. 2 difference, bands 2 & 9
Gaussian size distribution parameters and effective radius retrieved assuming ice-smoke mixture	chan. 2 difference, bands 2 & 9
Vertical ice water column abundance, or IWC ($g\ km^{-2}$)	band 9
Vertical optical depths (OD) for all wavelengths	chan. 2 difference, bands 2, 3, 4, 5, 8, 9, 10, 12, 14, & 15
Gaussian size distribution parameters retrieved from OD	chan. 2 difference & band 9

4.2.1. SOFIE Data Products Functional Description

SOFIE data products range from level 0 (L0) to L4, as described in Table 4.2-3. The SOFIE L2 results are also reported as a mission file, which includes one retrieval (e.g., H_2O) for the entire mission (e.g., 2007 - 2022). The mission files were created based on user feedback, and are the most popular way for the community to access SOFIE results.

Table 4.2-3. SOFIE data level definitions.

Data Level	Data Format	Brief Description	Source
Level 0 (L0)	MYSQL	The raw measurements, including radiometers, sun sensor, and housekeeping data.	GATS
Level 1 (L1)	MYSQL, NetCDF	The measurements processed to account for instrument artifacts (e.g. multiplexing), calibrations, registration in height, and placement on uniform grids in height.	GATS
Level 2 (L2)	MYSQL, NetCDF	Vertical profiles of all retrieved species and aerosol extinctions, in one file per day.	GATS
Mission Files (derived from L2)	NetCDF	Vertical profiles of each L2 species, reported in one file that spans the entire mission (i.e., May 2007 - present).	GATS
Level 3 (L3)	jpg image	Daily longitude vs. height cross-sections of each species, as a color contour image.	GATS
Level 4 (L4) AKA, PMC Summary File	NetCDF	Retrieved PMC physical properties such as ice mass density, particle size, ice temperature, ice particle axial ratio, and the content of meteor smoke in ice.	GATS

Level 4b (L4b) AKA, Gravity Wave File	NetCDF	Retrieved gravity wave parameters.	VT

4.2.2. SOFIE Science Data Distribution

The SOFIE Data Processing Center (SDP) includes personnel and facilities for processing, archiving and disseminating all SOFIE data. The SDC processes the SOFIE data from level 0 through the retrieval of geophysical science quantities (L2) and PMC microphysical properties (L4). The processing also includes analysis products such as gravity wave information [*Thurairajah et al.*, 2014] and PMC microphysical properties [*Hervig et al.*, 2009, 2012]. All products are validated by the SOFIE team, archived, and disseminated to the community via the SOFIE webpage (sofie.gats-inc.com). SOFIE data are also available on NASA's SPDF/HDP. The SPDF SOFIE interface includes all Levels 2 through 4, in addition to documentation and software.

4.3. CDE Science Data Products

This subsection details the science data products produced by the CDE instrument.

4.3.1. CDE Data Products Functional Description

CDE data processing software levels are as follows:

Level 0: Extracts the data from the CCSD packets.

Level 1: Separates the data by packet type, including science, housekeeping, calibration, and flash and SRAM memory dumps. These data are then put into the Level 1 database.

Level 2: Generates charge values from Level 1 DN values using the instrument calibration files.

Level 3: Converts charge to equivalent mass, removes noise using the reference detectors and other coincident events to produce validated IDP impact rates as function of dust mass.

Level 4: Calculated total influx in each hemisphere and determines monthly means with uncertainties.

CDE data products range from level 0 (L0) to L4, as described in Table 4.3-1.

Table 4.3-1. CDE data level definitions.			
Data Level	**Data Format**	**Brief Description**	**Source**
Level 0	ASCII	The raw measurements	LASP
Level 1	NetCDF	Time of impact, Pulse-height and engineering & housekeeping data	LASP
Level 2	NetCDF	Time of impact, and mass of the detected meteoroid.	LASP
Level 3	ASCII	Total meteoric mass per orbit, and impact rates per mass bin.	LASP
Level 4	ASCII	Meteoroid influx (# y^{-1} m^{-2}), as monthly means in each hemisphere.	LASP

4.3.2. CDE Science Data Distribution.

CDE L1 and L2 data are publicly available on the AIM webpage (aim.hamptonu.edu). Higher level data products are presented in the paper by *Poppe et al*. [2011], which describes the useful results obtained in 2007-2008 (it was deactivated in 2012). L4 data are available on the AIM webpage and on the SPDF, and are reproduced here in Table. 4.3.2. L3 data are not yet publicly available. CDE data are also available on NASA's SPDF/HDP. The SPDF CDE interface includes data Levels 1, 2, and 4, in addition to documentation and software.

Table 4.3.2. CDE L4 data.

AIM/CDE meteoroid influx
Results are monthly averages vs. time, in the Northern Hemisphere (NH) & Southern Hemisphere (SH)
See *Poppe et al.* [2011], PSS 59 (2011) 319-326, Figure 13, for details.
Note that the NH results appear to have a high bias, that is not yet understood. SH results agree with Wind observations [*Malaspina and Wilson*, 2016].

Date		Northern Hemisphere		Southern Hemisphere	
		Influx.	Sigma	Influx.	Sigma
m d y	yyyydoy	[# y^{-1} m^{-2}].		[# y^{-1} m^{-2}]	
6 15 07	2007166	10512.3	7405.7	-999	-999
7 15 07	2007197	5956.5	3599.2	142.5	94.6
8 15 07	2007228	6899.5	1999.8	673.5	134.2
9 15 07	2007258	7706.2	1763.1	2238.7	319.3
10 15 07	2007289	14319.3	4603.0	377.5	127.5
11 15 07	2007319	10721.7	4700.9	530.9	121.4
12 15 07	2007350	7835.7	3712.1	1489.5	296.8
1 16 08	2008016	7847.8	2152.5	1214.0	123.5
2 15 08	2008046	6093.9	953.6	3844.9	240.1

5. Ground System

The AIM project uses two complementary data systems, the Mission Operations Data System (MODS) and the SDS. The MODS consists of systems needed to command, control, and monitor the AIM spacecraft and instruments, and falls under the authority of the Mission Operations Manager at LASP / CU. Detailed definition and description of the MODS is outside the scope of this document. This document focuses on the SDS, which is responsible for processing the instrument data into data products useful to AIM program elements and other interested groups.

The functions of the AIM SDS are distributed over several facilities. SDS facilities also support functions that are not related to the data system. Only functions that are directly related to the routine production, acquisition, archival or distribution of data are within the scope of the SDS. Functions that pertain to satellite and/or instrument operations fall under the scope of the Mission Operations Data Systems (MODS) and are detailed in a separate document. The Mission Operations Manager at LASP / CU will coordinate these functions.

5.1. Ground System Architecture

The AIM SDS is a distributed system with elements that are part of several different facilities. These facilities are listed in Table 5.1. The AIM Mission Operations Center (MOC) is the central facility responsible for satellite operations and telemetry distribution. The instrument Payload Operations Center (POC) located at the instrument Data Processing Center (DPC) serves as the demarcation point between the MODS and the SDS. Only the portion of the POC involved with telemetry distribution falls within the scope of the SDS. The remaining portions fall within the scope of the MODS.

Table 5.1. AIM data system facilities.

Facility Name	**Location**
AIM Mission Operations Center (MOC)	LASP / CU
SOFIE Payload Ops & Data Processing Center (POC-DPC)	GATS
CIPS Payload Ops & Data Processing Center (POC-DPC)	LASP / CU
CDE Payload Ops & Data Processing Center (POC-DPC)	LASP / CU (inactive)
AIM Project Data Center (PDC)	Hampton University (HU)

5.2. AIM Mission Operations Center (MOC)

The AIM MOC is responsible for:

- Initial processing and distribution of spacecraft and instrument telemetry.
- Playback distribution of spacecraft and instrument telemetry.
- Archival (during the mission) of all raw and level 0 telemetry data.
- Maintaining planned and as-run timelines for spacecraft and instruments.

5.3. Instrument Payload Operations Center (POC)

Each instrument POC is responsible for:

- Supplying the MOC with instrument planning and as flown status information.
- Archiving the level 0 data for their instrument.
- Producing data quality assessments for their instrument.
- Producing instrument state of health information for short-term limits, configuration, long-term trends, and performance analysis.

5.4. Instrument Data Processing Center (DPC)

Each instrument DPC is responsible for:

- Producing, managing, and archiving the level 1-4 products for their instrument.
- Producing, managing, and archiving the survey data products for their instrument.
- Managing and archiving the analysis data products generated by the science team associated with their instrument.
- Providing necessary data processing support for the science team associated with their instrument.
- Supplying the PDC with data product metadata and generation status information.
- Disseminating the science data products for their instrument, as well as information and documentation pertaining to their instrument, to the scientific community and public.
- Supplying data product holdings to the DPC for inclusion in the final archive.
- Participating in the review of the final archive.

5.4.1. CIPS DPC

The CIPS DPC includes personnel and facilities for processing all CIPS data through the retrieved and value-added data products, and for producing CIPS data for distribution and archival. This includes code development at all levels, as well as code ingestion for high-level science products. The DPC is responsible for ensuring the integrity of all data products on a daily basis. It has been fully operational since May 23, 2007 and all planned data products are produced routinely). Data for levels 2 and higher are disseminated to the community via the CIPS webpage (http://lasp.colorado.edu/aim/). Data are produced and posted to the webpage on a daily basis, with a 6-day delay between data collection and definitive processing and distribution.

Cloud microphysical parameters are retrieved from the CIPS data via a three-step process [*Lumpe et al.*, 2013]. The level 0 data stream is first time-tagged, geolocated and calibrated to produce Level 1A images. This process is implemented separately for each of the four CIPS cameras. The next step is the Level 2 processing, which is the primary CIPS cloud retrieval process. The CIPS DPC has recently implemented a new CIPS Level 2 retrieval algorithm, v5.20. The primary objectives of this new version are to handle Continuous Imaging operations, correct some known residual image calibration errors, improve the data signal-to-noise and background subtraction, and enable detection and retrieval of dimmer clouds at lower latitudes than the previous version, which was v4.20. V5.20 has been in operational production for approximately five months and is stable. The CIPS DPC has reprocessed all CIPS data since the beginning of the mission using the v5.20 processing code. In addition to performing routine daily processing, the DPC continues to

perform all reprocessing, regression testing and quality control/validation for the new data products.

A new processing stream has been integrated into the DPC. This stream generates Level 2 and Level 3 RAA data products, which are entirely new CIPS science data products that are being used for GW studies. The data version for the new products is v1.10. This processing stream starts with the v5.10 Level 1A data and produces Level 2 RAA files for both scene-by-scene and full orbit strip data. A new level 2 RAA data product is the RAA variance. This data product will facilitate automated analysis of the RAA data, since it applies an FFT analysis to identify gravity waves, discriminating between the waves and other sources of variability. Variances have been calculated for all RAA observations since the beginning of the mission, and are currently under evaluation. In addition, the level 2 variance data will be combined to produce Level 3 daily global variance maps. The DPC will make these new products available to the science community immediately upon completion of internal validation studies by the CIPS team.

5.4.2. SOFIE DPC

The SOFIE DPC includes personnel and facilities for processing, archiving and disseminating all SOFIE data. The SDC processes the SOFIE data from level 0 through the retrieval of geophysical science quantities (L2) and PMC microphysical properties (L4). The processing also includes analysis products such as gravity wave information [*Thurairajah et al.*, 2014] and PMC microphysical properties [*Hervig et al.*, 2009, 2012]. All products are validated by the SOFIE team, archived, and disseminated to the community via the SOFIE webpage (sofie.gats-inc.com). The processing keeps up with the stream of new observations, and will reprocess all data when a new algorithm version comes online. The current SOFIE data version is available on the SOFIE webpage, and previous versions can be obtained via the SOFIE anonymous ftp site. The current publicly available SOFIE data are version 1.3 (V1.3), which have been processed and released to the public from May 2007 through November 2019.

Development of SOFIE V1.4 is currently nearing completion. The main changes are 1) altitude registration using measured refraction angles, 2) update nonlinearity calibration constants, 3) improved H_2O channel signal corrections, 4) improvements to NO retrievals including PMC corrections, 5) a merged O_3 retrieval covering the stratosphere and mesosphere, and 6) improved CO_2 retrievals. An error analysis of SOFIE CO_2 measurements revealed a direct dependence on the WACCM model CO_2 that is used for the altitude registration process. Briefly, the SOFIE altitude scale is re-positioned in height by comparing the measured CO_2 transmission at 25-35 km to simulations based on NCEP T/P and WACCM CO_2. Testing revealed that this procedure induced a 1-to-1 link between the WACCM and retrieved CO_2 VMR. This unwanted dependence was eliminated in V1.4 results by conducting an altitude registration where the measured refraction angles are compared to simulations based on NCEP T/P (which are independent of assumed gas mixing ratios). With this new algorithm in place, the SOFIE CO_2 retrievals are now ready for scientific use. V1.4 testing is nearly complete and public data release will occur in the next months.

SOFIE data collection and processing has required modifications due to the changing AIM orbit beginning in late 2015. The main change was a reduction in the solar sink rate (from ~3 km s^{-1} to less than 1 km s^{-1}) due to the increased angle between the orbit plane and Earth – Sun vector (beta angle). The lower sink rates were easily accommodated by increasing the SOFIE event duration from 150 to 400 s. SOFIE originally performed an automated gain setting procedure that gave electronic difference signals balanced to a specified level. This procedure occurred at a set time relative to event start, and the reduced solar sink rates would have caused the balance

procedure to occur at atmospheric heights and contaminate some of the science data. This occurred during May – August 2015, and was successfully remedied on the ground through algorithm modifications. To address the issue on orbit, the procedure was terminated in favor of constant gain settings, also in September 2015. This approach was taken because the relative times were hard-coded, and years of SOFIE data indicated nearly constant gain settings (from the automated procedure) in all 16 bands. The approach is working satisfactorily to date. Implementing the two changes in SOFIE operations required the upload of a new event table, and an additional ground contact to accommodate the increased SOFIE file size.

5.5. AIM Project Data Center (PDC)

The AIM PDC hosts the AIM website and currently acts as host for the preliminary archive. The AIM website, http://aim.hamptonu.edu, contains general information about AIM, news releases, publications, and links to more in-depth information on the spacecraft and instruments. Orbit information is available along with a tool for predicting ground overpasses. Automated weekly predictions of AIM overpasses are available to the public. Documentation on the mission, instruments, calibrations, and data products are available directly from the AIM website.

Currently, data files from the SSDC and CSDC are pushed to the PDC as soon as they have been approved by the respective instrument PI for public release. The Space Physics Data Facility (SPDF) pulls these files from the PDC. Data from the SOFIE instrument is processed typically within 1 week, made available to the public on the SSDC, pushed to the PDC, and pulled by the SPDF. Data from the CIPS instrument is processed typically within 2 days of acquisition. This CIPS data is made available to the public on the CSDC, pushed to the PDC and pulled by the SPDF, but it is labeled "preliminary". This is because the CIPS data processing requires calibrations that must be completed near each equinox before the data products are considered "definitive". After the definitive processing of the data is completed, the definitive data files are pushed to the PDC and pulled by the SPDF. During FY2023 the CIPS and SOFIE Science Data centers will take over the delivery of data to the SPDF with no changes to the above approach and cadence.

6. Data Flow

6.1. Overview of End-to-End Data Flow

The SDS is responsible for the acquisition, generation, distribution, and archival of science data necessary to support the AIM mission. In this capacity, the SDS provides useful data products to the AIM program elements, the scientific community, K-14 educators and the general public (Figure 6.1).

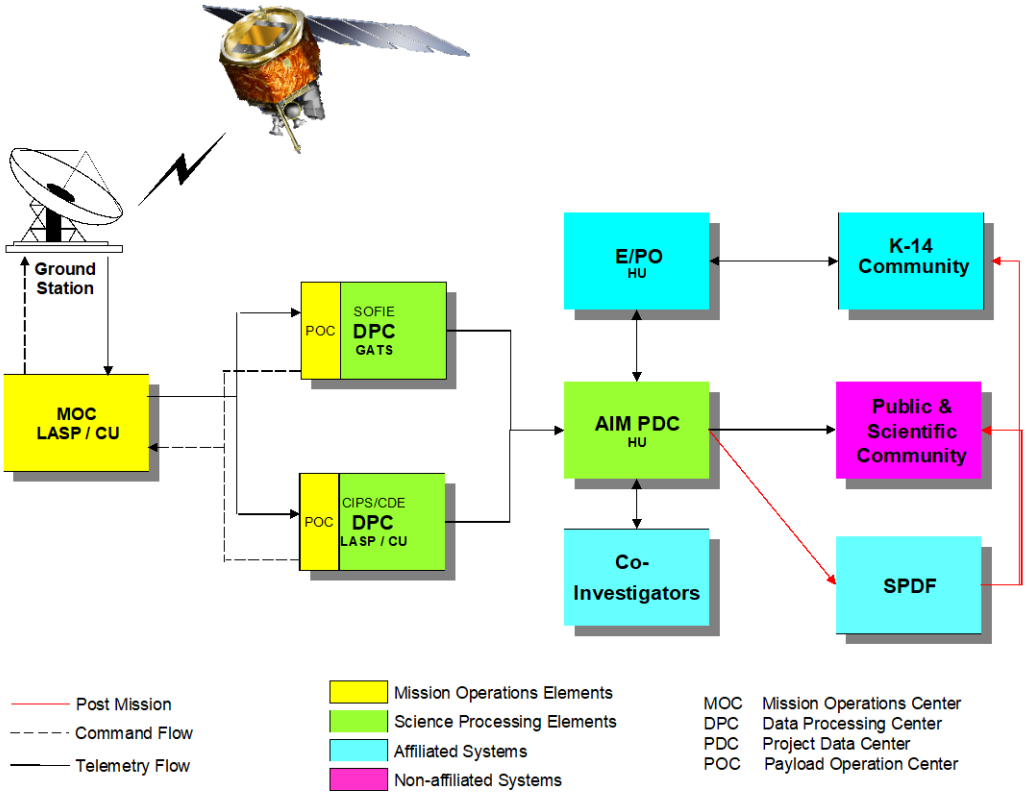

Figure 6.1. AIM Science Data System shows the various AIM program elements and external users of the SDS. The SDS supplies data to both AIM program elements and external users. Beginning in FY2023 the DPCs will be the primary means of data access to the public, the team, and the SPDF.

6.1.1. Data Flow to Spacecraft

See Section 2.2.2 for details on the AIM Mission Operations Center (MOC) structure and logistics. Due to command issues which were first encountered very early in the mission, the AIM spacecraft has been fully automated to perform its routine orbital science acquisition. Therefore, modifications to the desired observation have been predominantly done to mitigate for the

changing orbital parameters (altitude, beta-angle, orbital precession), and therefore only exchanges between the Science Operations Centers and the Mission Operation Center are performed. The Mission Operations Manager routinely attends Science Team telecons and meetings to keep abreast of the changing observational needs. SOFIE modifications are developed by GATS and delivered to the MOC in a ready to uplink format. CIPS modifications are developed by the DPC. Because of the command issues, many of these uplinks have been performed using AIM's alternative commanding method, which requires the MOC to reformat instrument command requests to be compatible with that operation. When regular commanding can be accomplished, both SN and GN resources are scheduled (about one contact per orbit or more), and command loads are reformatted for autonomous uplink whenever a command opportunity occurs. Otherwise, the SN is used for alternative commanding using institutional capabilities that are not available via the GN.

6.1.2. Data Flow from Spacecraft

Transmitter performance has been nominal, with no issues noted. The transmitter is left on continuously and the downlink regularly returns to the TDRSS/low rate mode after every high rate ground station pass.

The following actions take place after data are received at the ground station:

1. The telemetry service function (at the MOC) distributes portions of the telemetry (Level 0 data) to the POC-DPCs and mission operations. This distribution can take place in both near-real time and in playback mode.
2. The Level 0 data are used at the POCs and mission operations for planning, command and assessment purposes. These functions are not within the scope of the SDS, however results of planning and assessment activities will serve as input to the SDS. Communications between mission operations and the command and assessment function of the POCs are not within the scope of the SDS.
3. Level 0 data, as well as planning and assessment products, are used to generate routine data products. This takes place at the MOC, the POCs, and DPCs. These products will be served by their producers. All communications required for product generation are within the scope of the SDS. Preliminary data products and images are typically available within 24-48 hours after the observations, subject to verification by the instrument science team. After initial calibrations at the beginning of each PMC season, a more definitive data product is provided within 6-7 days (after definitive ephemeris information is obtained).
4. The products resulting from product generation are archived at the various facilities. These archives are used by the science teams for data analysis. Data analysis activities are not within the scope of the SDS. However, results of data analysis (data analysis products) will be transferred from the science teams into the appropriate archive.
5. Access to AIM data by the science community (including AIM users), K-14 educators, and the general public is provided via the Internet at each SDC. Each AIM SDC facility maintains a web and ftp site serving the data products generated by that facility.
6. As data is processed, all data products that are made publicly available as well as level 1 and higher products that were used in their generation are transferred to the SPDF The SPDF synchronizes their data with the interim archive on a nightly basis.

6.2. Data Handling and Timeline

Table 6.2 summarizes the flow of data from the spacecraft as well as the transfer method along with the timeline for delivery to/from each element. Table 6.2 summarizes the flow of data from the spacecraft as well as the transfer method along with the timeline for delivery to/from each element.

Table 6.2. Data flow timeline.

Flow	Data Product	Timeline	Transfer Method
MOC to POC/DPC	Science data products	< 1 week	rsync over ssh
DPC to PDC	Science data products	<1 day from being made publicly available. Typically < 1 week from initial data-taking once seasonal calibrations have been completed.	rsync over ssh
DPC to SPDF	Science data products	nightly synchronization	rsync over ssh

7. Archiving and Data Access

7.1. Current Archive Locations

AIM science data products are generated and stored at each individual instrument Science Data Center (SDC). The CIPS SDC is located at U C Boulder LASP, and the SOFIE SDC is located at GATS, inc. The SDCs also make these products available to the public via their websites: http://lasp.colorado.edu/aim/ and http://sofie.gats-inc.com/sofie/index.php. Fully calibrated level 2 and higher data is released without any access requirements. The SDCs are responsible to transmit all science data products level 1 and higher when they are processed and fully calibrated to the interim archive at Hampton University. The SPDF mirrors the SDC archives and makes available the level 2 and higher products without access restrictions via the Heliophysics Data Portal (HDP). The SPDF is responsible for the long-term archiving of the AIM data.

7.2. Data Access and Processing Tools

The AIM data products are provided in NetCDF format and are therefore accessible using many standard NetCDF readers for various analysis toolkits. As a reference, Interactive Data Language (IDL)-based tools to read and plot the released data are also provided and will be stored in the Final Archive. They are currently available via the web at: http://aim.hamptonu.edu/library/tools/index.html. The AIM SDS also provides other Web-based tools to the scientific community to facilitate the analysis of AIM data. Web-based tools for previewing the data are hosted by the individual SDC facilities. After mission completion, these web based

tools will continue to be provided as part of the Resident Archive, but will not be included in the Final Archive.

7.3 Documentation and Metadata

Documentation for the AIM data products is provided by the individual instrument DPCs as part of the archiving process. The final list of documents to be included will be determined by the DPCs at mission close, however during the mission it will be available on the DPC websites and stored in a documentation sub-directory for each instrument within the interim and final archives. Software tools included in the documentation directories of the archives are intended for reference only, not as fully supported and operational software suites.

The AIM metadata scheme is based largely upon the metadata for the TIMED mission and is generally compatible with the SPASE data model. The AIM metadata provides the SPASE equivalent of Numerical Data, Display Data, and some Catalog data at the "granule" and "physical parameter" levels. AIM metadata has been made available in a format used by the Virtual Ionosphere Thermosphere Mesosphere Observatory (VITMO) and usable by other Virtual Observatories.

Table 7.3. AIM Instrument and Data Product Documentation

Document	Description	Last Updated
cips_data_overview.pdf	Overview of CIPS data products	2020-04-28
cips_instrument_overview.pdf	Overview of CIPS instrument	2020-04-28
cips_level1a.pdf	CIPS Level 1A Data	2011-05-02
cips_level2.pdf	CIPS Level 2 PMC Data	2014-07-23
cips_level2_raa.pdf	CIPS Level 2 RAA Data	2017-06-02
cips_level3a.pdf	CIPS Level 3A Data	2011-12-28
cips_level3C_v4.pdf	CIPS Level3C Data , v4.20r06	2020-03-15
cips_level3C_v5.pdf	CIPS Level3C Data, v5.20	2020-03/15
cips_level3d.pdf	CIPS Level 3D Data	2012-01-10
cips_level3e.pdf	CIPS Level 3E Data	2012-05-31
AIM_CDE_ATBD.doc	CDE Algorithm Theoretical Basis Document	2004-10-19
cde_level_1_product_details.doc	CDE Level 1 Data	2007-12-18
cde_level_2_product_details.doc	CDE Level 2 Data	2007-12-18
CDE_PSR_Science_and_Calibration-James.ppt	PSR presentation of CDE calibrations	2005-10-6

CDE_SDC Algorithm Structure.ppt	CDE processing algorithm overview	2006-01-31
cde_sdc_calibrations.doc	formal description of CDE calibrations	2006-02-02
SOFIE_atbd_V1.1.doc	SOFIE Algorithm Theoretical Basis Document	2008-02-07
SOFIE_CalibrationEventsDescription_V1.0.doc	Explanation of the pointing requirements for the s/c and AIM Planning & Scheduling folks for on-orbit calibration events.	2007-05-19
SOFIE_Calibration_Product_Summary_V1.8.doc	Describes dark current, FOV, boresight, relative spectral response, gain calibration, and non-linearity studies	2011-01-11
SOFIE_l1_netcdf_file_description_V1.0.doc	SOFIE Level 1 Data	2008-02-08
SOFIE_l2_netcdf_file_description_V1.02.doc	SOFIE Level 2 Data	2008-02-07
SOFIE_Level3_Product_Description_V1.0.doc	SOFIE Level 3 Data	2008-02-05
SOFIE_Level0b_to_level1_icd_V1.0.doc	Interface Control document between the SOFIE Level0b and SOFIE Level 1 processing.	2008-02-07
SOFIE_Level0b_Design_Review_V1.0.ppt	Overview of the SOFIE Level0b software design.	2008-02-05

7.4. Final Archive/Mission Archive Plan

The Space Physics Data Facility (SPDF) has been designated as the long-term archive for the AIM mission data. The SPDF will be responsible for maintaining and serving the AIM data only after mission closeout. Access to the AIM data products and documents are provided by the instrument SDCs. Data products are collected by the PDC and placed in the appropriate archive format for the SPDF. In FY2023 the SPDF will begin to collect data directly from the SDCs. The AIM Science Team will determine the contents of the archive. The baseline long-term archive contents are as follows:

- The most current version of the data products and associated metadata files.
- Preview images for data products in PNG format.
- Summary files in ASCII or other appropriate format.
- Mission documentation and status data products.
- Algorithm Theoretical Basis Documents.

• Support products available only through the AIM program.

• Utility software for data display and processing.

• Bibliography of AIM related publications.

Depending on reprocessing activities throughout the mission, several versions of the processed data will be made available through the AIM SDS as part of the Mission Archive. As versions of the AIM data are made publicly available through the AIM SDS, it will also be copied to the final mission archive. Deprecated data sets may be removed from the final archive when superseded by newer versions of the data. This process is currently active and provides both a proof of the processes for transfer of final mission products to the final mission archive at the end of mission, and a backup in case of catastrophic loss of data within the AIM SDS prior to the end of mission.

7.4.1. Data Products

At the end of mission a final review of the data products to be archived will be conducted by each instrument DPC. Prior to that review, as part of the ongoing archiving effort, the current data products will be transferred from the instrument DPCs to the final archive. As per NASA requirements, this list includes data from Level 1 and higher. Level 0 and lower data products are not required by NASA for archive. Level 1 data products are the highest level that has not been irreversibly transformed. Level 2 and higher data products contain retrieved parameters that are of use to the scientific community. During the mission it is expected that only level 2 data and higher will be made publicly available. Table 7.4.1 contains the current list of data products being archived and their formats. A more detailed description of each can be found in individual instrument subsections in section 4 of this project data management plan.

Table 7.4.1. Current AIM archive data products and summary files.

Data Product	**Data Format**
CIPS Level 1a	NetCDF
CIPS Level 2 PMC-only	NetCDF and png
CIPS Level 3a PMC-only	NetCDF and png
CIPS Level 3b PMC-only	mp4
CIPS Level 3c PMC-only	IDLsave and ascii(v4) or NetCDF(v5)
CIPS Level 3d PMC-only	ascii
CIPS Level 3e PMC-only	ascii
CIPS Level 2a RAA-only	NetCDF and png
CIPS Level 2b RAA-only	NetCDF and png
CIPS Level 2c RAA-only	png
CIPS Level 3a RAA-only	NetCDF and png
SOFIE Level 1	NetCDF
SOFIE Level 2	NetCDF
SOFIE Level 2 Mission Files	NetCDF
SOFIE Level 3	jpg image
SOFIE Level 4 (AKA, PMC Summary File)	NetCDF
SOFIE Level 4b (AKA, Gravity Wave File)	NetCDF

CDE Level 1	ASCII
CDE Level 2	NetCDF
CDE Level 3	NetCDF
CDE Level 4	ASCII

7.4.2. Analysis Tools

The AIM data products are provided in NetCDF format and are therefore accessible using many standard NetCDF readers for various analysis toolkits. As a reference, Interactive Data Language (IDL) based tools to read and plot the released data are also provided and will be stored in the Final Archive. Additional reference tools in other programming languages may be added to the archive as they become available. These tools will be included within the documentation section of the final archive. The AIM SDS also provides other Web-based tools to the scientific community to facilitate the analysis of AIM data. Web-based tools for previewing the data are hosted by the individual SDC facilities. After mission completion, these tools will continue to be provided as part of the Resident Archive, but will not be included in the Final Archive.

7.4.3. Documentation

Each instrument DPC is responsible for producing and managing the documentation for the data products produced by their facility. Documentation for individual data products are unlikely to require significant changes outside of major software revisions. During the mission, each DPC as part of their archiving responsibility will include all documentation relevant to the data that is being sent to the final archive. At the end of mission as part of the final review of the data products that will be included in the final archive, each DPC will conduct a review of existing documentation and identify all documentation that corresponds to the data in the final archive.

7.4.4. Final Archive Access and Distribution

The NASA Space Physics Data Facility (SPDF) has been designated as the long-term archive for the AIM mission data. The SPDF will be responsible for maintaining and serving the AIM data, tools, and documentation after mission closeout.

8. References

DeLand, M. T., E. P. Shettle, G. E. Thomas, and J. J. Olivero (2006a), A quarter-century of satellite PMC observations, *J. Atmos. Solar-Terr. Phys.*, *68*, 9-29, doi:10.1016/j.jastp.2005.08.003.

DeLand, M. T., E. P. Shettle, G. E. Thomas and J. J. Olivero (2006b), Spectral measurements of PMCs from SBUV/2 instruments, *J. Atm. Sol.-Terr. Phys*., *68*, 65-77, doi:10.1016/j.jastp.2005.08.006.

DeLand, M. T., E. P. Shettle, G. E. Thomas, and J. J. Olivero (2007), Latitude-dependent long-term variations in polar mesospheric clouds from SBUV version 3 PMC data, *J. Geophys. Res*., 112, D10315, doi:10.1029/2006JD007857.

Fiedler, J., G. Baumgarten, and G. von Cossart (2005), Mean diurnal variations of noctilucent clouds during 7 years of lidar observations at ALOMAR, *Ann. Geophys., 23(4)*, 1175–1181.

Fiedler, J., G. Baumgarten, U. Berger, P. Hoffmann, N. Kaifler, and F.-J. Lübken (2011), NLC

and the background atmosphere above ALOMAR, *Ann. Geophys.*, *11*, 5701-5717, doi:10.5194/acp-11-5701-2011.

Fentzke, J. T., and D. Janches (2008), A semi-empirical model of the contribution from sporadic meteoroid sources on the meteor input function in the MLT observed at Arecibo, *J. Geophys. Res., 113*, A03304, doi:10.1029/2007JA012531.

Garcia, R. R. (1989), Dynamics, radiation, and photochemistry in the mesosphere: Implications for the formation of noctilucent clouds, *J. Geophys. Res., 94*, 14605-14,615, doi:10.1029/JD094iD12p14605.

Gordley, L. L., M. Hervig, C. Fish, J. M. Russell III, S. Bailey, J. Cook, S. Hansen, A. Shumway, G. Paxton, L. Deaver, T. Marshall, J. Burton, B. Magill, C. Brown, E. Thompson, and J. Kemp, The Solar Occultation For Ice Experiment (SOFIE) (2009), *J. Atmos. Solar-Terr. Phys.*, *71*, 300-315, doi:10.1016/j.jastp.2008.07.012.

Hervig, M. E., R. E. Thompson, M. McHugh, L. L. Gordley, J. M. Russell III, and M. E. Summers (2001), First confirmation that water ice is the primary component of polar mesospheric clouds, *Geophys. Res. Letters, 28*, 971-974.

Hervig, M.E., L.L. Gordley, M. Stevens, J.M. Russell, S. Bailey, and G. Baumgarten (2009), Interpretation of SOFIE PMC measurements: Cloud identification and derivation of mass density, particle shape, and particle size, *J. Atmos. Solar-Terr. Phys.*, *71*, 316-330, doi:10.1016/j.jastp.2008.07.009.

Hervig, M. E., L. L. Gordley, L. E. Deaver, D. E. Siskind, M. H. Stevens, J. M. Russell III, S. M. Bailey, L. Megner, and C. G. Bardeen (2009), First satellite observations of meteoric smoke in the middle atmosphere, *Geophys. Res. Letters*, doi:10.1029/2009GL039737.

Hervig, M. E., L. E. Deaver, C. G. Bardeen, J. M. Russell, S. M. Bailey, and L. L. Gordley (2012), The content and composition of meteoric smoke in mesospheric ice particles from SOFIE observations, *J. Atmos. Solar-Terr. Phys.,* http://dx.doi.org/10.1016/j.jastp.2012.04.005.

Hervig, M. E., U. Berger, D. E. Siskind (2016a), Decadal variability in PMCs and implications for changing temperature and water vapor in the upper mesosphere, *J. Geophys. Res.*, 121, 2383-2392, doi:10.1002/2015JD024439.

Hervig, M. E., Brooke, J. S. A., Feng, W., Bardeen, C. G., Plane, J. M. C. (2017a), Constraints on meteoric smoke composition and meteoric influx using SOFIE observations with models, *J. Geophys. Res. Atmospheres, 122*, doi:10.1002/2017JD027657.

Hervig, M. E., C. G. Bardeen, D. E. Siskind, M. J. Mills, R. Stockwell, (2017b), Meteoric smoke and H_2SO_4 aerosols in the upper stratosphere and mesosphere, *Geophys. Res. Letters, 44*, doi:10.1002/2016GL072049.

Hervig, M. E., Plane, J. M. C., Siskind, D. E., Feng, W., Bardeen, C. G., & Bailey, S. M. (2021). New global meteoric smoke observations from SOFIE: Insight regarding chemical composition, meteoric influx, and hemispheric asymmetry. *Journal of Geophysical Research: Atmospheres, 126*, e2021JD035007. https://doi. org/10.1029/2021JD035007.

Hervig, M. E., D. Malaspina, V. Sterken, L. B. Wilson III, S. Hunziker, S. M. Bailey (2022), Decadal and annual variations in meteoric flux from Ulysses, Wind, and SOFIE observations, *J. Geophys. Res. Space Physics,* in review.

Horányi, M., Hoxie, V., James, D. et al. (2008), The Student Dust Counter on the New Horizons Mission, *Space Sci Rev 140*, 387–402. https://doi.org/10.1007/s11214-007-9250-y.

Horz, F., Brownlee, D.E., Fechtig, H., Hartung, J.B., Morrison, D.A., Neukum, G., Schneider, E., Vedder, J.F., Gault, D.E. (1975), Lunar microcraters: Implications for the micrometeoroid

complex, *Planet. Space Sci. 23*, 151–172.

Janches, D., and D. O. ReVelle, The Initial Altitude of the Micrometeor Phenomenon: Comparison between Arecibo radar observations and theory, *J. Geophys. Res.*, *110*, art. no.-A08307, 2005.

Karlsson, B., Kornich H., and J. Gumbel (2007), Evidence for interhemispheric stratosphere-mesosphere coupling derived from noctilucent cloud properties, *Geophys. Res. Letters*, *36*, 34, L16806, doi:10.1029/2007GL030282.

Leslie, R., Sky glows, *Nature*, 32, 245 (1885).

Leinert, C. (1975), Zodiacal light - A measure of the interplanetary environment, *Space Sci. Rev. 18*, 281–339.

Love, S. G., and D. E. Brownlee (1993), A direct measurement of the terrestrial mass accretion rate of cosmic dust, *Science*, *262*, 550-553.

Lumpe, J.D., S.M. Bailey, J.N. Carstens, C.E. Randall, D.W. Rusch, G.E. Thomas, K. Nielsen, C. Jeppesen, W.E. McClintock, A.W. Merkel, L. Riesberg, B. Templeman, G. Baumgarten, J.M. Russell, IlI (2013), Retrieval of polar mesospheric cloud properties from CIPS: algorithm description, error analysis and cloud detection sensitivity, *J. Atmos. Solar-Terr. Phys*, 104, 167-196, http://dx.doi.org/10.1016/j.jastp.2013.06.007.

Malaspina, D. M. and L. B. Wilson III (2016), A database of interplanetary and interstellar dust detected by the Wind spacecraft, *J. Geophys. Res. Space Physics, 121*, 9369–9377, doi:10.1002/2016JA023209.

Mathews, J. D., D. Janches, D. D. Meisel, and Q. H. Zhou, The micrometeoroid mass flux into the upper atmosphere: Arecibo results and a comparison with prior estimates, *Geophys. Res. Lett.*, *28*, 1929, 2001.

McClintock, William, D.W. Rusch, G.E. Thomas, A.W. Merkel, M.R. Lankton, V.A. Drake, S.M. Bailey, and J.M. Russell III, The Cloud Imaging and Particle Size experiment on the Aeronomy of Ice in the Mesosphere mission: Instrument concept, design, calibration, and on-orbit performance, J. Atmos. Solar-Terr. Phys., doi:10.1016/j.jastp.2008.10.011, 2009.

Nalwa, H.S., 1995. Ferroelectric Polymers. Marcel Dekker, Inc.

Poppe, A., Jacobsmeyer, B., James, D., Horaányi, M., 2010. *Nucl. Instrum. Methods A622*, 583–587.

Poppe, A., James, D., Horányi, M. (2011), Measurements of the terrestrial dust influx variability by the Cosmic Dust Experiment, *Planetary and Space Sci., 59*, 319-326, doi:10.1016/j.pss.2010.12.002.

Randall, C. E., et al. (2017), New AIM/CIPS global observations of gravity waves near 50–55 km, *Geophys. Res. Lett.*, 44, 7044– 7052, doi:10.1002/2017GL073943.

Russell, J. M. III, S. M. Bailey, M. Horányi, L. L. Gordley, D. W. Rusch, M. E. Hervig, G. E. Thomas, C. E. Randall, D. E. Siskind, M. H. Stevens, M. E. Summers, M. I. Taylor, C. R. Englert, P. J. Espy, W. E. McClintock and A. W. Merkel, Aeronomy of Ice in the Mesosphere (AIM): Overview and early science results, *J. Atmos. Solar-Terr. Phys.*, doi:10.1016/j.jastp.2008.08.011, 2009.

Schwanenthal, J.P., 2004. Debris in-orbit evaluator (DEBIE) calibration and data analysis. Ph.D. Thesis, The Open University.

Simpson, J.A., Tuzzolino, A.J. (1985), Polarized polymer films as electronic pulse detectors of cosmic dust particles, *Nucl. Instrum. Methods A 236*, 187–202.

Sparks, J. J., and Janches, D. (2009), Latitudinal dependence of the variability of the micrometeor

altitude distribution, *Geophys. Res. Lett., 36*, L12105, doi:10.1029/2009GL038485.

Stevens, M. H., et al. (2012), Bright polar mesospheric clouds formed by main engine exhaust from the space shuttle's final launch, *J. Geophys. Res.*, doi:10.1029/2012JD017638.

Sparks, J. J., and Janches, D. (2009), Latitudinal dependence of the variability of the micrometeor altitude distribution, *Geophys. Res. Lett., 36*, L12105, doi:10.1029/2009GL038485.

Taylor, M. J., M. Gadsden, R. P. Lowe, M. S. Zalcik, and J. Brausch (2002), Mesospheric cloud observations at unusually low latitudes, J. Atmos. Sol. Terr. Phys., 65, doi:10.1016/S1364-6826(02)00053-6.

Thomas, G. E. (1996), Is the polar mesosphere the miner's canary of global change?. *Adv. Space Res., 18*, 149-158, doi: 10.1016/0273-1177(95)00855-9.

Thurairajah, B., S. M. Bailey, C. Y. Cullens, M. E. Hervig, and J. M. Russell III (2014), Gravity wave activity during recent stratospheric sudden warming events from SOFIE temperature measurements, *J. Geophys. Res. Atmos., 119*, 8091–8103, doi:10.1002/2014JD021763.

Tuzzolino, A.J. (1992), PVDF copolymer dust detectors: particle response and penetration characteristics, *Nucl. Instrum. Methods A 316*, 223–237.

Tuzzolino,A.J.,etal. (2001a), The Space Dust (SPADUS) instrument aboard the Earth-orbiting ARGOS spacecraft: I—instrument description, *Planet Space Sci, 49*, 689–703, https://doi.org/10.1016/S0032-0633(01)00012-5.

Tuzzolino, A.J., et al. (2001b), The Space Dust (SPADUS) instrument aboard the Earth-orbiting ARGOS spacecraft: II–results from the first 16 months of flight, *Planet. Space Sci., 49*, 705–729, https://doi.org/10.1016/S0032-0633(01)00013-7.

Tuzzolino, A.J., et al. (2004), Dust Measurements in the Coma of Comet 81P/Wild 2 by the Dust Flux Monitor Instrument, *Science, 304*, 1776–1780.